Article

Neuron

Mouse Motor Cortex Coordinates the Behavioral Response to Unpredicted Sensory Feedback

Highlights

- Motor cortex (M1) is necessary for the motor response to an unexpected perturbation
- M1 is not necessary when the same movement is carried out spontaneously
- Layer 2/3 neurons are differentially activated by unexpected visual perturbations
- Activity in layer 5 PT neurons correlates with behavioral responses

Authors

Matthias Heindorf, Silvia Arber, Georg B. Keller

Correspondence

silvia.arber@unibas.ch (S.A.), georg.keller@fmi.ch (G.B.K.)

In Brief

The role of motor cortex in movement control is controversial. Heindorf et al. demonstrate that motor cortex mediates corrective behavioral responses to unexpected visual perturbations, paralleled by layer-specific cortical responses distinct from the ones during the same movement without perturbation.

Heindorf et al., 2018, Neuron *99*, 1040–1054
September 5, 2018
https://doi.org/10.1016/j.neuron.2018.07.046

CellPress

CellPress

Neuron
Article

Mouse Motor Cortex Coordinates the Behavioral Response to Unpredicted Sensory Feedback

Matthias Heindorf,[1,2] Silvia Arber,[1,2,4,*] and Georg B. Keller[1,3,4,5,*]
[1]Friedrich Miescher Institute for Biomedical Research, 4058 Basel, Switzerland
[2]Biozentrum, Department of Cell Biology, University of Basel, 4056 Basel, Switzerland
[3]Faculty of Natural Sciences, University of Basel, 4056 Basel, Switzerland
[4]These authors contributed equally
[5]Lead Contact
*Correspondence: silvia.arber@unibas.ch (S.A.), georg.keller@fmi.ch (G.B.K.)
https://doi.org/10.1016/j.neuron.2018.07.046

SUMMARY

Motor cortex (M1) lesions result in motor impairments, yet how M1 contributes to the control of movement remains controversial. To investigate the role of M1 in sensory guided motor coordination, we trained mice to navigate a virtual corridor using a spherical treadmill. This task required directional adjustments through spontaneous turning, while unexpected visual offset perturbations prompted induced turning. We found that M1 is essential for execution and learning of this visually guided task. Turn-selective layer 2/3 and layer 5 pyramidal tract (PT) neuron activation was shaped differentially with learning but scaled linearly with turn acceleration during spontaneous turns. During induced turns, however, layer 2/3 neurons were activated independent of behavioral response, while PT neurons still encoded behavioral response magnitude. Our results are consistent with a role of M1 in the detection of sensory perturbations that result in deviations from intended motor state and the initiation of an appropriate corrective response.

INTRODUCTION

In mammals, movement is controlled by circuits spanning throughout the central nervous system from the cortex to the spinal cord, where motor neurons orchestrate the contraction of the many different body muscles. While the activity of neurons closer to motor output correlates well with muscle contraction, the relationship between activity and movement is less clear in higher level motor circuits. In motor cortex, neuronal activity correlates with a diverse range of parameters including speed of movement (Beloozerova and Sirota, 1993a), direction (Georgopoulos et al., 1986), muscle activity (Armstrong and Drew, 1984), movement error signals (Inoue et al., 2016), or was proposed to follow a dynamic attractor (Churchland et al., 2012). Different lines of research provide evidence that motor cortex impacts on motor output. Perhaps most strikingly, stimulation of motor cortex, either electrically or optogenetically, results in muscle contractions (Brecht et al., 2004; Ferrier, 1874; Harrison et al., 2012; Miri et al., 2017; Tennant et al., 2011). These effects could be mediated by direct projections from motor cortex to the spinal cord. Layer 2/3 motor cortex neurons are recurrently connected and provide intracolumnar excitatory drive to layer 5 pyramidal tract (PT) neurons (Weiler et al., 2008). Layer 5 PT neurons project ipsilaterally to other regions involved in motor control such as striatum and the basal pontine nucleus (Jankowska and Edgley, 2006; Kita and Kita, 2012). Given that feedback connectivity from layer 5 PT neurons to more superficial neurons is sparse (Kiritani et al., 2012; Morishima and Kawaguchi, 2006), this suggests that layer 2/3 neurons function to integrate cortical input (Huber et al., 2012) and coordinate the activation of layer 5 PT neurons, which in turn influence behavioral output circuits.

Interpretations on a prominent role of motor cortex in movement control and motor learning, however, are complicated by the fact that motor cortex lesions result in different behavioral phenotypes across species. In non-human primates and humans in particular, motor cortex lesions abolish most capacity for movement that recovers with training in non-human primates (Lang and Schieber, 2003; Murata et al., 2008; Zaaimi et al., 2012). Similar lesions in rodents, however, result in no overt movement impairment (Kawai et al., 2015). Hence, although motor cortex is directly connected to many subcortical circuit components, it remains unclear under which circumstances and/or for what types of movements cortical control is exerted on these circuits. Reliance on motor cortex might be stronger for dexterous movements that require precise feedback control. Movement control could thus rely on motor cortex during conditions in which processing of sensory information also relies on cortex. Mouse visual cortex, for example, is thought to not only process visual information, but also act as a detector of visual feedback that deviates from the visual feedback based on motor output (Attinger et al., 2017; Fiser et al., 2016; Zmarz and Keller, 2016). Consistent with the hypothesis that motor cortex might be involved in the processing of deviations of expected from actual sensory input, selective responses triggered by unexpected feedback perturbations during locomotion are present in cat

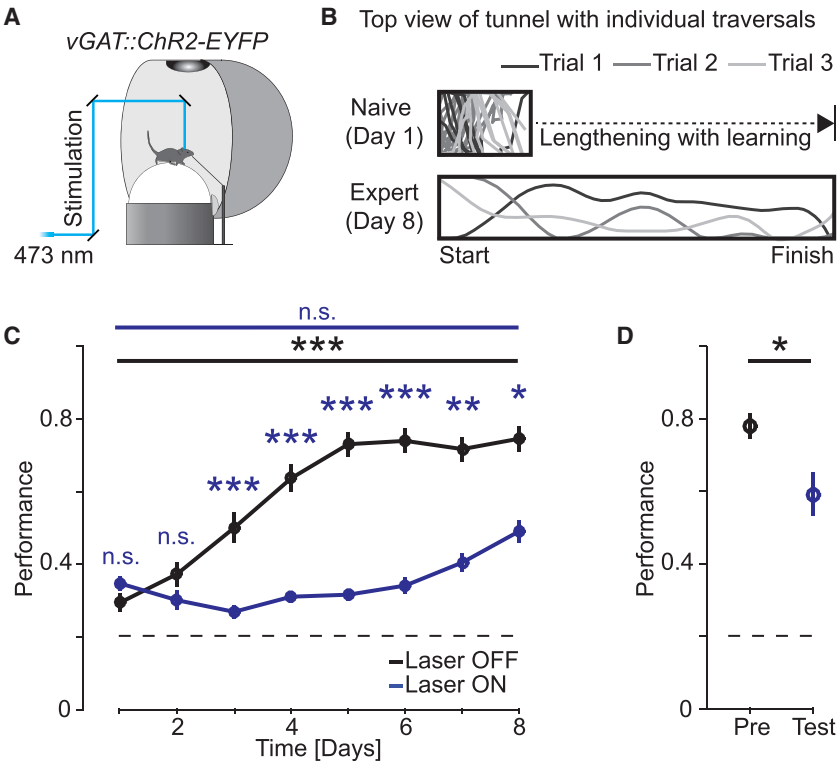

Figure 1. Performance in a Visually Guided Virtual Reality Navigation Task Is Motor Cortex Dependent

(A) Mice were trained to control movement in a virtual environment through locomotion on the spherical treadmill. Upon reaching the target at the end of the corridor, mice received a water reward. A blue laser was directed at left and right motor cortex in rapid alternation for optogenetic inhibition of neuronal activity via excitation of vGAT+ interneurons.

(B) Top: schematic of the tunnel with three example traversals at the beginning of training (day 1, tunnel is not drawn to scale, length-to-width ratio: 5:1). Bottom: schematic of the tunnel with three example traversals from an expert mouse (day 8). With increasing performance of the mice, we increased the length of the tunnel to increase the difficulty of the task (length-to-width ratio: 30:1).

(C) Average performance as a function of training days (fraction of time spent running in the direction of the target, see STAR Methods) in mice with (blue, n = 12 mice) and without (black, n = 22 mice) motor cortex inhibition. Here, data from all three groups of mice with different inhibition laser power levels (1 mW, 2 mW, and 10 mW) are pooled (see also Figure S1E). Error bars indicate SEM over mice. Dashed black line marks chance performance. *$p < 0.05$, **$p < 0.01$, ***$p < 10^{-3}$; Wilcoxon rank sum test. Mice trained with photoinhibition did not significantly improve performance as opposed to the control group (day 1 versus day 8; with photoinhibition: $p = 0.17$, n = 12 mice; without photoinhibition: $p < 10^{-6}$, n = 22 mice; Wilcoxon rank sum test).

(D) Photoinhibition decreased performance in expert mice (n = 15 mice). *$p < 0.05$; Wilcoxon rank sum test. Error bars indicate SEM over mice. Dashed black line marks chance performance.

motor cortex (Marple-Horvat et al., 1993), and in rodents it has been shown that motor cortex is necessary for the rapid initiation of a behavioral response to an unexpected feedback perturbation (Lopes et al., 2016). Moreover, exposing animals to increased demands for movement accuracy results in increased activity in motor cortex, which could be the consequence of increased precision in sensory feedback guided control of movement (Beloozerova et al., 2010; Beloozerova and Sirota, 1993b; Farrell et al., 2015). It is thus conceivable that motor cortex is particularly relevant for generating an appropriate behavioral response to deviations from expected sensory information.

To investigate the role of motor cortex in sensory guided coordination of movement, we trained mice to navigate to a target at the end of a virtual corridor in the presence of unexpected shifts in the direction of the corridor. We show that motor cortex inhibition interferes with both task learning and execution. By recording calcium signals in layer 2/3 and layer 5 PT neurons, we found that activity in both populations changed in a learning-dependent manner and correlated with the amplitude of individual turns mice make while navigating. In response to an unexpected shift of the corridor, mice executed corrective turns. Surprisingly, we found that under these conditions, neuronal activation in layer 2/3 did not depend on the subsequent behavioral response. This is consistent with the idea that during consolidation of a motor skill, layer 2/3 integrates signals from other cortical areas while layer 5 becomes successively more involved in the control of movement with learning.

RESULTS

Involvement of Motor Cortex in the Feedback Guided Control of a Spherical Treadmill

To investigate how motor cortex is involved in visually guided motor control, we trained mice to navigate to a target at the end of a corridor by controlling turning and forward movement for a water reward in a virtual reality environment while head-fixed on an air-supported spherical treadmill (see STAR Methods, Figure 1A, and Video S1). Task performance was quantified as the fraction of time mice spent running in the target direction (within an angle of ±36°, chance performance is 20%) normalized by the total time spent running. We made the task more difficult with increasing performance of the mice by progressively lengthening the virtual tunnel throughout training to keep the number of rewards per training session approximately constant (Figure 1B). Mice typically performed above chance level already in the first session and on average reached plateau performance by session 6 (5.3 ± 1.5 sessions, mean ± standard deviation, n = 22 mice) (Figure 1C).

We first determined whether the anterior part of primary motor cortex that contains the caudal forelimb area (CFA) (Harrison

et al., 2012; Tennant et al., 2011) implicated in the control of forelimbs is involved in execution. We did this by bilateral optogenetic inhibition either throughout training or once mice reached plateau performance. We implanted cranial windows over left and right motor cortices in transgenic mice that express channelrhodopsin-2 in inhibitory neurons (*vGAT::ChR2(H134R)-EYFP*), a strategy previously used successfully to inhibit neuronal activity in cortex (Guo et al., 2014). The laser spot had a diameter of 0.8 mm (full width at half maximum) at the surface of cortex and was moved bilaterally to either one (1.5 mm lateral and 0.5 mm anterior of bregma) or two locations (1.5 mm lateral, and 0.5 mm and 1.5 mm anterior of bregma) during the scan (Figure S1A). Mice were trained either with motor cortex inhibited throughout the first eight training sessions at three different levels of inhibition (1 mW, 2 mW, and 10 mW laser power; n = 12 mice; see STAR Methods) or under non-inhibited conditions (n = 22 mice). In absence of motor cortex inhibition, mice increased task performance significantly over the course of the first eight training sessions. In contrast, mice that received motor cortex inhibition during training showed impaired learning (Figures 1C, S1B, and S1C). The amount of impairment depended on the level of inhibition (laser power) and the extent of the cortical area inactivated (Figures S1A and S1D). The effects of inactivation of CFA were stronger than those observed with inactivation of a more anterior location in M1 (Figures S1A and S1E). Inactivation effects were likely not simply a consequence of the transient nature of optogenetic inhibition, as a similar impairment in task learning was observed in a different group of mice (n = 5 mice) that received small bilateral ibotenic acid lesions targeted to CFA prior to training (Figures S1D and S1F). These data demonstrate that motor cortex and in particular CFA activity is necessary for learning of the task. We then continued training two groups of mice (3 mice previously trained with chronic motor cortex inhibition and 3 mice without motor cortex inhibition) for another six training sessions without motor cortex inhibition. Performance of mice that had received chronic inhibition of motor cortex in the initial eight training sessions increased to a performance level matching that of normally trained mice, at a learning rate not different from initial learning in mice without motor cortex inhibition (Figure S1G). Subsequent inhibition of motor cortex in expert mice resulted in a significant decrease in performance (Figure 1D). To ensure that laser stimulation alone did not interfere with performance, we trained four mice that did not express channelrhodopsin-2 with laser stimulation of motor cortex and found no impairment in learning (Figure S1H). Taken together, these results demonstrate that motor cortex is necessary for both learning and execution of a virtual navigation task that requires visually guided control of a spherical treadmill.

To perform this virtual navigation task, mice learn to control left and right corrective turns to steer toward a target while running on the spherical treadmill using visual feedback. Peak velocity and acceleration of these spontaneous turns increased over the course of training (Figures 2A and 2B; day 1 versus day 8, speed: $p < 10^{-4}$, acceleration: $p < 10^{-5}$, n = 22 mice; Wilcoxon rank sum test). We selected turns based on a threshold on the rotational velocity of the treadmill. To include only well isolated turns, we discarded turns that were preceded by another turn in the same direction within less than 5 s (see STAR Methods). To test whether motor cortex inhibition interferes with the ability to execute turns, we compared turning behavior with and without motor cortex inhibition. We found no evidence for an effect of motor cortex inhibition on the amplitude of spontaneous turns in expert mice during performance testing days (Figures 2C and 2D). We next tested whether the frequency with which mice executed turns was influenced by motor cortex inhibition. We found that inhibition of motor cortex only led to a modest reduction in the frequency of spontaneous turns (number of turns per second of time spent running without optogenetic inhibition was: 0.12 ± 0.009, mean ± SEM; and with optogenetic inhibition: 0.10 ± 0.014, mean ± SEM; n = 15 mice; p = 0.07; Wilcoxon rank sum test, see STAR Methods), and at the same time resulted in a small increase in locomotion speed (11.4 cm/s ± 3.5 cm/s [mean ± SD, n = 12 mice] with inhibition, versus 7.8 cm/s ± 2.6 cm/s [mean ± SD, n = 12 mice] without inhibition; p = 0.02; Wilcoxon rank sum test). Thus, motor cortex inhibition did not reduce the overall vigor of movement or impair the mouse's ability to execute spontaneous turns.

Given that motor cortex inhibition did not affect the general ability to run and turn on the ball, but nevertheless significantly reduced task performance, we argued that motor cortex might be necessary for the coordination of visually guided movements. Mice continuously detect deviations from intended heading and correct for these deviations by executing turns. Spontaneous turns can be executed either under visual guidance, and thus correct for course deviations, or independent of visual guidance. To obtain better experimental control of when mice initiate visually guided turns, we introduced sudden and unexpected visual offsets (Video S2). Mice are then required to respond to an immediate and unexpected perturbation in their visual field in order to correct for a course deviation. We first tested whether mice respond to these visual offset perturbations, and whether these induced turns require motor cortex.

Unexpected visual offset perturbations were implemented by suddenly shifting the heading of the mouse in the virtual corridor by 30° either to the left or right at a random time during corridor traversal (see STAR Methods). To prevent any potential interference with initial task learning, we did not introduce perturbations in the first two days. We found that mice typically responded to perturbations with a rapid corrective turn (Figure 2E). Fully trained mice responded with a corrective response within 1 s of the offset in 74% ± 4% (mean ± SEM, n = 14 mice) of trials. The latency of the first detectable turning response following the visual offset perturbation was 301 ms ± 45 ms (mean ± SEM, n = 19 mice). As with spontaneous turns, the speed and acceleration of these induced turns increased over the course of training (Figure 2F, $p < 0.002$; n = 22 mice; Wilcoxon rank sum test). Hence, mice rapidly detect and correct for visual offset perturbations.

To probe for the involvement of motor cortex in these rapid corrections in response to unexpected visual perturbations, we quantified the effect of motor cortex inhibition on induced turns. In mice with chronic motor cortex inhibition during training, responses to visual offset perturbations were strongly reduced (fraction of trials with a corrective response: 28% ± 2%, mean ± SEM, n = 12 mice; Figures S2A and S2B). We then tested the effect of brief (3 s) inhibition of motor cortex concurrent with

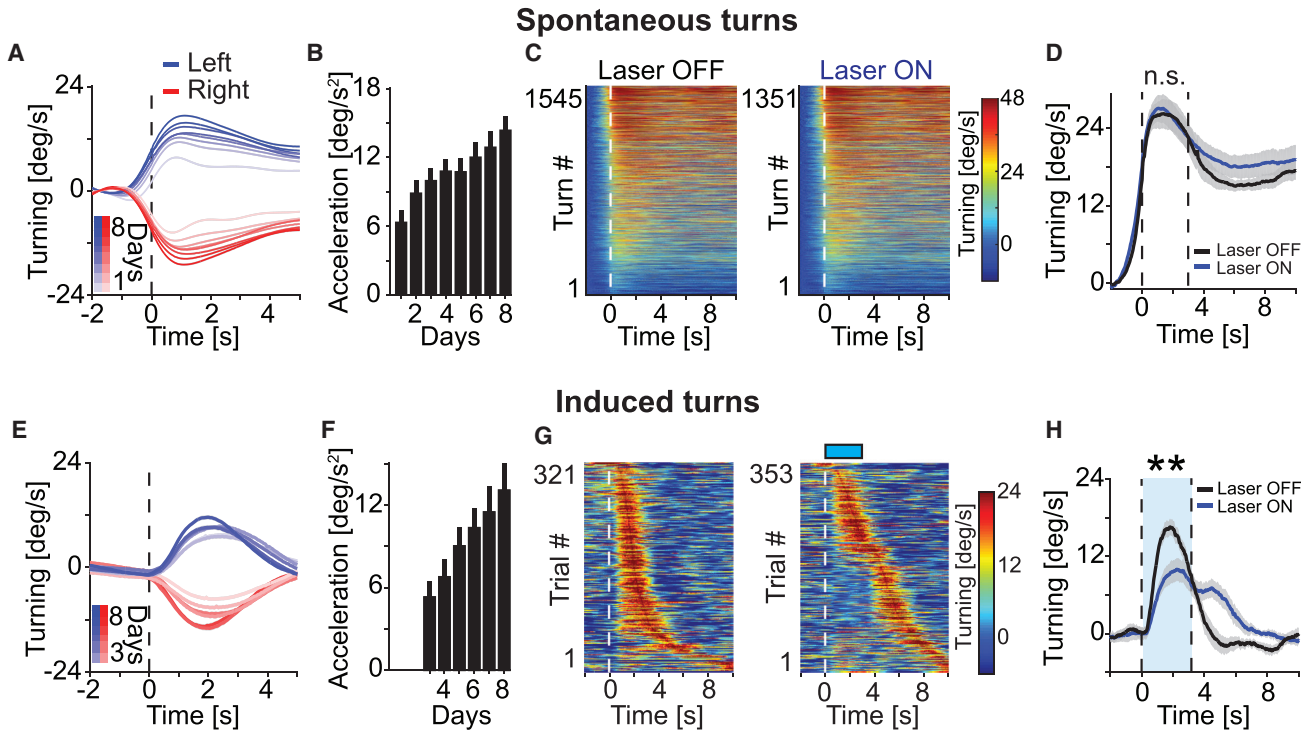

Figure 2. Motor Cortex Inhibition Delays Visually Guided Corrective Turns

(A) Mice spontaneously turn left and right as they learn to traverse the virtual corridor. The amplitude of spontaneous turns increased over the course of training (days 1 to 8) for both left (blue) and right (red) turns. Shading indicates SEM over turns. Turns per day, left: 184 ± 27; right: 186 ± 28 (mean ± SD, n = 22 mice).

(B) Average acceleration during spontaneous turns increased with training ($p < 10^{-8}$, $R^2 = 0.19$, n = 22 mice; linear trend analysis; see STAR Methods). Error bars indicate SEM over mice (n = 22 mice).

(C) Speed profiles of the spontaneous turns without inhibition of motor cortex (left panel, n = 14 mice) and the spontaneous turns initiated during inhibition of motor cortex (right panel, n = 14 mice, data from the same mice as in left panel), executed on performance testing days in expert mice, sorted by maximum speed. Motor cortex inhibition did not prevent mice from executing spontaneous turns. Color indicates turning speed.

(D) Average speed profile of turns without (black) and with (blue) bilateral inhibition of motor cortex. Same data as shown in (C). Shading indicates SEM over mice (n = 14 mice). Note that turning speed with or without motor cortex inhibition was not different in a window 3 s after turn onset (marked by dashed lines). n.s., not significant; Wilcoxon rank sum test.

(E) Average speed profiles during corrective turns to the left (blue) and right (red) induced by visual offset perturbations over the course of training (days 3 to 8, the first 2 days did not have visual offset perturbations, left turns: n = 632, 666, 688, 803, 776, 884; right turns: 675, 687, 725, 806, 749, 907 in 22 mice, respectively). Shading indicates SEM over turns. Turns per day, left: 34 ± 4; right: 34 ± 4 (mean ± SD).

(F) Acceleration during corrective turns induced by visual offset perturbations increased over the course of training ($p < 10^{-5}$, $R^2 = 0.15$, n = 22 mice; linear trend analysis; see STAR Methods). Error bars indicate SEM over mice (n = 22 mice).

(G) Speed profile of 321 visual offset perturbation-induced corrective turns in expert mice that had reached plateau performance without (left panel, n = 14 mice, data from same mice as in C) and with (right panel, 353 trials, n = 14 mice, data from the same mice as in left panel) inhibition of motor cortex concurrent with visual offset perturbation for 3 s (blue bar). Turns are sorted by latency to peak velocity. In a subset of trials (55% ± 5%, mean ± SEM, see STAR Methods), mice delayed their corrective turn response until after motor cortex inhibition ceased. Color indicates turning speed.

(H) Average speed profile of visual offset perturbation-induced corrective turns without (black) and with (blue) bilateral inhibition of motor cortex for 3 s starting concurrently with the visual offset perturbation (time 0). Same data as shown in (G). Shading indicates SEM over mice (n = 14 mice). Turning speed was lower with motor cortex inhibition (0 s – 3 s after perturbation onset). **p < 0.01; Wilcoxon rank sum test.

visual offset perturbations in trained mice (n = 14 mice that all had at least eight training sessions preceding the test session). With motor cortex inhibition concurrent with visual offset perturbations, mice were less likely to execute a corrective turn within 1 s of the visual offset (45% ± 5%, mean ± SEM, Figures 2G and 2H). This effect was less pronounced when inactivating the more anterior region of M1 only (Figures S2C and S2D). In trials in which the inhibition of motor cortex prevented a corrective turn within 1 s of the visual offset, mice typically executed a corrective turn immediately after cessation of motor cortex inhibition. The fraction of trials without a corrective turn depended on the timing of the onset of the motor cortex inhibition relative to the perturbation. When the onset of motor cortex inhibition preceded the visual offset perturbation by 1 s or occurred concurrently, the fraction of trials without corrective response was significantly larger than when inhibition onset followed the perturbation onset by 1 s (Figures S2E and S2F). This analysis was confounded by the fact that mice transiently reduced forward locomotion speed concurrent with the onset of motor cortex inhibition. However, mice reduced locomotor speed both in trials with and without delayed turning response (Figure S2G), indicating that the delayed turning response cannot be explained by the reduction in

locomotion speed. Finally, we ensured that the inhibition of the turning response was mediated by activation of channelrhodopsin-2 in cortical interneurons and not a consequence of the laser stimulation itself. In mice that did not express channelrhodopsin-2, laser stimulation had no effect on the probability of a corrective turn (Figures S2H and S2I).

In summary, we found that motor cortical activity is necessary for visually guided turn execution, but not for the execution of a turn per se. Chronic motor cortex inhibition prevented responses to visual offset perturbations almost completely, and brief inhibition coincident with the visual offset perturbation significantly reduced the probability of mice executing a corrective turn. These results are consistent with the interpretation that motor cortex activity is necessary for the execution of a corrective movement in response to perturbation.

Activity in Motor Cortex Scaled Linearly with the Amplitude of Spontaneous Turns

To further investigate the role of motor cortex in task performance, we next recorded neuronal activity in CFA motor cortex (Figure S1A) chronically throughout training in either layer 2/3 or layer 5 PT neurons using two-photon calcium imaging of GCaMP6f (Chen et al., 2013) (Figure S3). We identified layer 2/3 neurons by recording depth and using an AAV2/1-EF1α-GCaMP6f virus (1,154 neurons in 8 mice). For recordings of layer 5 PT neurons, we used a genetic and viral intersectional strategy with an AAV2/1-EF1α-DIO-GCaMP6f in *Sim1(KJ18)-Cre* mice (Gerfen et al., 2013) (560 neurons in 11 mice). Layer 5 PT neurons are thought to have the most direct impact on movement control (Kita and Kita, 2012; Li et al., 2015). The transfer function from neuronal activity to calcium signal in these genetically encoded calcium indicators is non-linear, but monotonic. As a consequence, single spikes may not always be detectable and our activity measures are biased toward bursts of neural activity. Moreover, the fluorescence change in response to an action potential across cell types, which may have different calcium buffering kinetics, may not be directly comparable. For this reason, we do not compare the magnitude of the calcium responses across cell types but instead compared how responses within one cell type change with time or as a function of behavioral variables.

We first analyzed neuronal responses during spontaneous turns (Figures 3A and 3B). We found that a substantial fraction of neurons had significant responses during spontaneous turns (mean ± SD, 49% ± 19% in 8 mice in layer 2/3, 39% ± 16% in 11 mice in layer 5 PT). We then split turns into contra- and ipsiversive depending on whether the turn was in the opposite or same direction as the hemisphere from which we recorded neuronal activity. We classified neurons as either more responsive during contraversive or ipsiversive turns (Table S1). To determine the population responses to turns, we first averaged the response of contraversive neurons to contraversive turns and the response of ipsiversive neurons to ipsiversive turns and averaged these two responses to a population response (see STAR Methods). To quantify neuronal response strength as a function of turn amplitude, we split turns into bins with different acceleration magnitudes and quantified neuronal responses of layer 2/3 neurons and layer 5 PT neurons as a function of turn acceleration. We found that activity in both layer 2/3 and layer 5 PT neurons scaled linearly with turn acceleration (Figures 3C–3J; layer 2/3: $p < 10^{-10}$, $R^2 = 0.08$, n = 1,154 neurons; layer 5 PT: $p < 10^{-10}$, $R^2 = 0.04$, n = 560 neurons; linear trend analysis, see STAR Methods). This scaling of neuronal response with increasing turn acceleration was present both early and late in training (Figures S4A and S4B). To test whether such a linear relationship between neuronal activity and acceleration of movement would exist for any movement, we analyzed responses during running onsets and split them by acceleration of running onset. We found no evidence of a linear relationship between neuronal activity and acceleration magnitude at running onset for either layer 2/3 or layer 5 PT neurons (Figures S4C–S4H). In summary, neuronal activity in mouse motor cortex increased linearly with turn acceleration. In contrast, although running onset resulted in a detectable increase in neuronal activity, this response did not linearly increase with acceleration.

With Learning, Neuronal Activity Decreased in Layer 2/3 and Increased in Layer 5 PT Neurons

Motor learning has been shown to alter neuronal activity in motor cortex in a variety of paradigms (Huber et al., 2012; Masamizu et al., 2014; Peters et al., 2017). To determine how turning-related responses change with learning, we compared spontaneous turning responses of the same neurons early (days 1 to 4) and late (days 5 to 8) during training, regardless of the neurons' preferred turning direction. We found that responses in layer 2/3 early in training were larger during contraversive turns than during ipsiversive turns. Late in training, the response during contraversive turns had decreased and was no longer different from the response during ipsiversive turns (Figures 4A and 4B; early versus late, contraversive: $p < 10^{-4}$; contraversive versus ipsiversive, early: p = 0.02, late: p = 0.52; n = 1154 neurons; paired Student's t test). In contrast, activity in layer 5 PT neurons increased selectively during contraversive turns, while, similar to the activity in layer 2/3 neurons, response amplitude during ipsiversive turns remained unchanged with training (Figures 4D and 4E; early versus late, contraversive: $p < 0.002$, ipsiversive: p = 0.89; n = 560 neurons; paired Student's t test). The bias of response strength of layer 5 PT neurons to contraversive turns was already present during the early phase but increased further with training (Figure 4E; contraversive versus ipsiversive, early: $p < 10^{-4}$, late: $p < 10^{-5}$; n = 560 neurons; paired Student's t test). Consistent with the increased layer 5 PT neuron activity over the course of training, we also found an increase in correlation with turning velocity in layer 5 PT, but not in layer 2/3 neurons (Figures 4C and 4F; early versus late, layer 2/3: p = 0.73; n = 1,154 neurons; layer 5 PT: $p < 10^{-17}$; n = 560 neurons; paired Student's t test). We then quantified the stability of neuronal responses during contra- and ipsiversive turns in layer 2/3 and layer 5 PT neurons by correlating the population response vector during contra- and ipsiversive turns across different days. We found that the neuronal representation was most stable in layer 5 PT neurons during contraversive turns with a time constant of 13.6 days, which was higher than during ipsiversive turns and higher than both contra- and ipsiversive response stability of layer 2/3 activity (Figure S5; layer 5 PT contraversive: 13.6 days, layer 5 PT ipsiversive: 6.9 days, layer

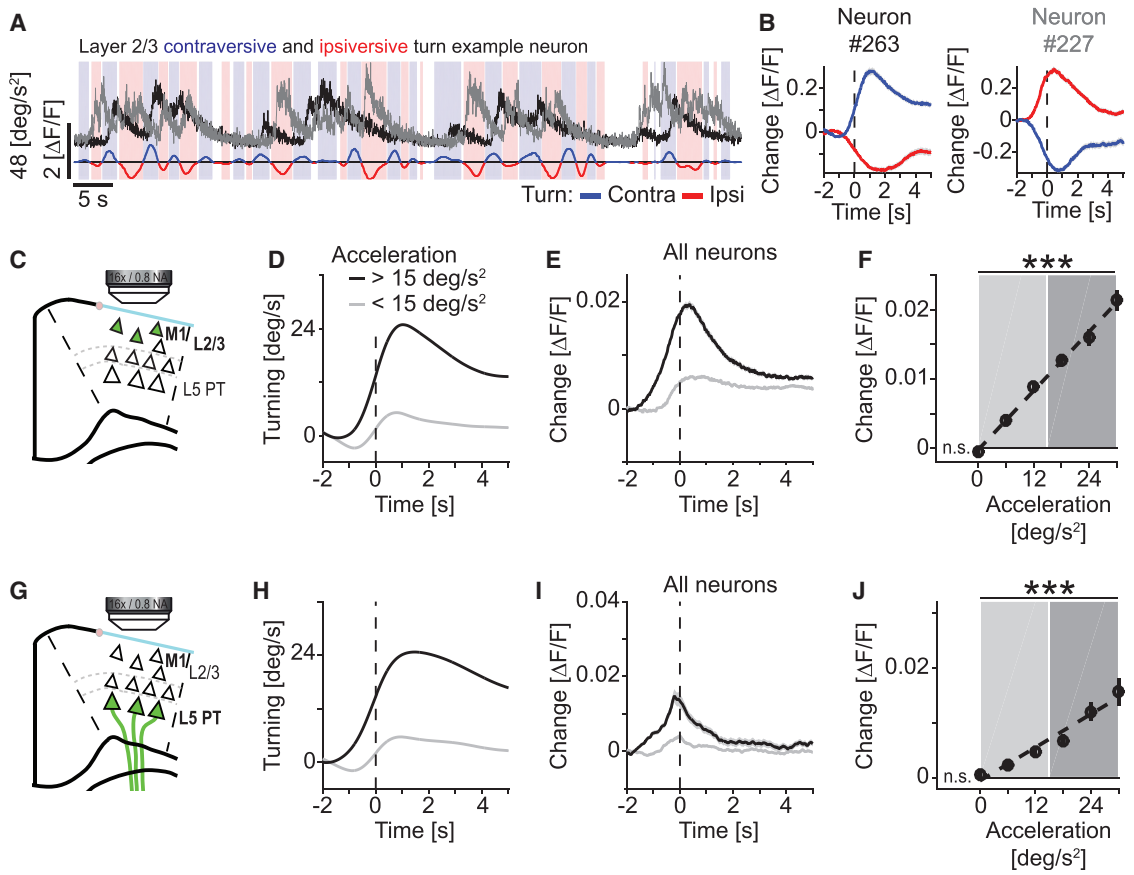

Figure 3. Calcium Response of Layer 2/3 and Layer 5 PT Neurons in Motor Cortex Scales Linearly with Amplitude of Spontaneous Turns

(A) Top: calcium activity of one layer 2/3 neuron that was preferentially active during contraversive turns (black line) and one layer 2/3 neuron that was preferentially active during ipsiversive turns (gray line). Bottom: the mouse's rotational acceleration. Times of positive acceleration mark contraversive turns (blue line and shading) and negative values mark ipsiversive turns (red line and shading).

(B) Average change in fluorescence aligned on contraversive (blue) and ipsiversive (red) turns throughout training (days 1 to 8) for the two neurons shown in (A). Shading indicates SEM over turns (number of contraversive turns: n = 1,654; ipsiversive turns: n = 1,668).

(C) To record the activity of layer 2/3 excitatory neurons, we injected AAV2/1-EF1α-GCaMP6f into *vGAT-Cre x ROSA-LSL-tdTomato* mice (n = 8).

(D) We split all spontaneous turns recorded throughout training (days 1 to 8) into bins of high (black line) and low (gray line) acceleration. Shading indicates SEM over turns (number of turns for high acceleration bin: n = 6,174; low acceleration bin: n = 14,018).

(E) Larger turns were associated with higher neuronal activity. Average population activity of layer 2/3 neurons for the turns shown in (D) (n = 1,154 neurons). Colors as in (D). Shading indicates SEM over neurons.

(F) Average population activity of layer 2/3 neurons as a function of acceleration of the spontaneous turn. Error bars indicate SEM over neurons (n = 1,154). Dashed black line is a linear fit to the data. Shading marks bins used for the turning and activity traces in (A) and (B). ***$p < 10^{-3}$, $R^2 = 0.08$, n = 1,154 neurons; linear trend analysis (see STAR Methods). n.s., not significant, lowest bin is not different from zero; Student's t test.

(G) To record the activity of layer 5 PT neurons, we injected conditional AAV2/1-DIO-EF1α-GCaMP6f into *Sim1(KJ18)-Cre* mice (n = 11 mice).

(H) As in (D), but for the layer 5 PT experiments (number of turns for high acceleration bin: n = 5,764; low acceleration bin: n = 21,865).

(I) As in (E), but for layer 5 PT neurons (n = 560 neurons).

(J) As in (F), but for layer 5 PT neurons. ***$p < 10^{-3}$, $R^2 = 0.04$, n = 560 neurons; linear trend analysis (see STAR Methods).

2/3 contraversive: 3.3 days, layer 2/3 ipsiversive: 4.6 days). Thus, activation during spontaneous turns was experience dependent in both layer 2/3 and layer 5 PT neurons, the changes in activity patterns with training exhibit opposing trends in the two cell types and the response stability across training was higher in layer 5 PT neurons.

Given that motor cortex inhibition selectively impeded the mouse's ability to successfully correct for visual offset perturbations, we speculated that motor cortical neurons might be activated more strongly during turns directed toward the target than during turns taken away from the target. To test for a differential activation of layer 2/3 and layer 5 PT neurons during turns toward compared to turns away from the target, we analyzed turn responses of both groups of neurons as a function of heading direction relative to the target preceding the analyzed turn. We found that activation of both layer 2/3 and layer 5 PT neurons was higher during turns that were taken toward the target (Figures 5 and S6). In summary, activation of motor cortical neurons was stronger when mice executed target-directed turns compared to when they executed turns away from the target.

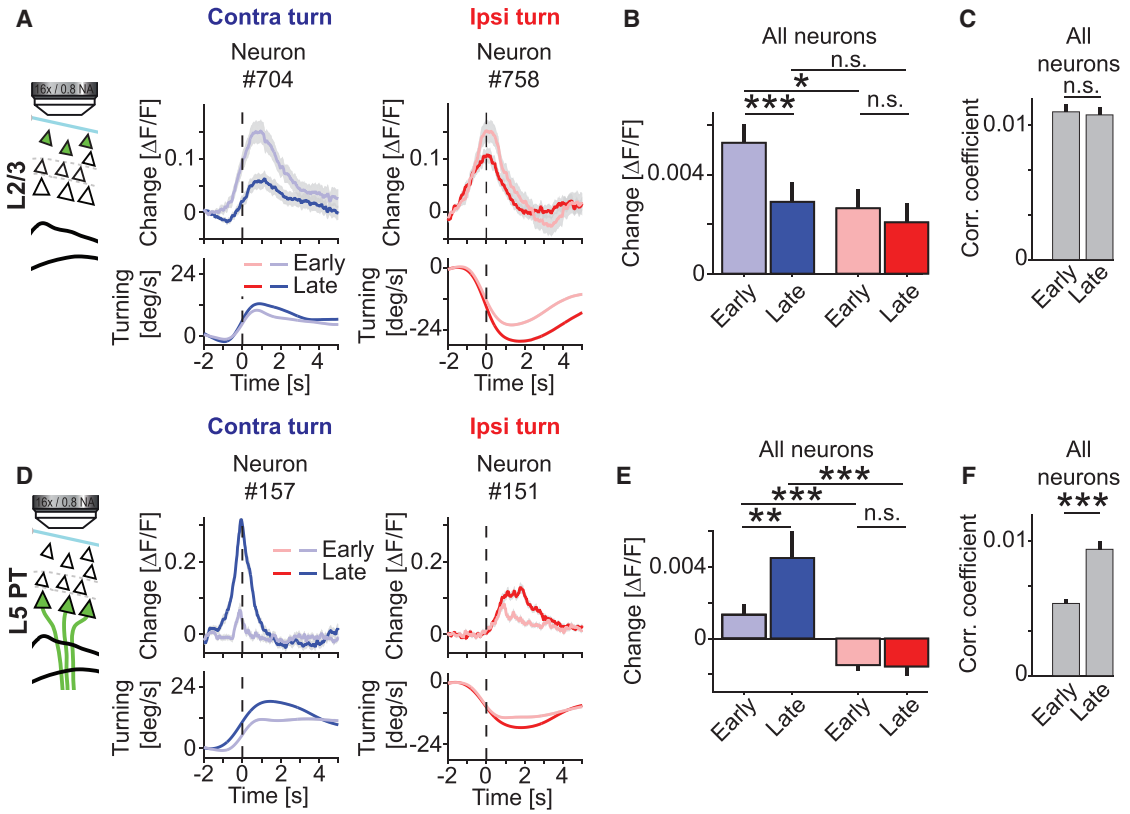

Figure 4. With Training Activity in Layer 2/3 Decreases and Increases in Layer 5 PT Neurons

(A) Top: average turn response of a layer 2/3 neuron during a contraversive turn (left) during the first 4 days of training (early, pale blue, n = 804 turns) and the last 4 days of training (late, dark blue, n = 818 turns); and the average turn responses of another neuron during ipsiversive turns (right) early (pale red, n = 819 turns) and late (dark red, n = 873 turns) in training. Bottom: average turning speed traces corresponding to the data shown in the top panels. Shading indicates SEM over turns.

(B) Average layer 2/3 responses during contraversive (blue) and ipsiversive (red) turns early (days 1 to 4) and late (days 5 to 8) in training. Responses during contraversive turns decrease with training. Error bars indicate SEM over neurons (n = 1,154 neurons). *p < 0.05, ***p < 10^{-3}, n.s., not significant; paired Student's t test.

(C) Average absolute Pearson's correlation coefficient of layer 2/3 activity and turning velocity early (days 1 to 4) and late (days 5 to 8) in training. n.s., not significant; paired Student's t test.

(D) As in (A), but for two layer 5 PT neurons (number of early contraversive turns: n = 592; late contraversive turns: n = 898; early ipsiversive turns: n = 590 turns; late ipsiversive turns: n = 899).

(E) As in (B), but for layer 5 PT neurons (n = 560 neurons). **p < 0.01, ***p < 10^{-3}, n.s., not significant; paired Student's t test.

(F) As in (C), but for layer 5 PT neurons. ***p < 10^{-3}; paired Student's t test.

Visual Offset Perturbations Activate Layer 2/3 Independent of Motor Response Magnitude

Given that motor cortex inhibition significantly reduced the ability of mice to respond to visual offset perturbations, we tested whether the responses of layer 2/3 and layer 5 PT neurons during induced turns differed from those during spontaneous turns. Both layer 2/3 and layer 5 PT neurons exhibited an increase of mean activity following the visual offset perturbation. The latency between visual offset perturbation and average neural response was 225 ms ± 54 ms (mean ± SEM, n = 8 mice) in layer 2/3 neurons and 283 ms ± 50 ms (mean ± SEM, n = 11 mice) in layer 5 PT neurons. In addition, turn-responsive neurons whose activation preceded the turn onset responded earlier in layer 2/3 than in layer 5 PT (layer 2/3: 176 ms; n = 190 neurons; layer 5 PT: 221 ms; n = 34 neurons; p = 0.01; Student's t test, see STAR Methods). We split the different visual offset trials into six bins by the rotational acceleration of the induced turn (Figures 6A–6C). Surprisingly, we found that layer 2/3 neurons responded to perturbations independent of the amplitude of the subsequent turn (Figures 6B and 6C). We found no evidence for a difference in response amplitude between trials on which mice executed no course correction on average and trials during which they exhibited maximal course correction in response to the visual offset perturbation (Figure 6C; first versus last bin, p = 0.71; n = 1,154 neurons; paired Student's t test). By contrast, the activation of layer 5 PT neurons reflected the magnitude of the subsequent turn. We found that in layer 5 PT neurons, there was a significant increase of neuronal responses with higher amplitudes of the turning magnitude (Figures 6D–6F; first versus last bin, p < 10^{-3}; n = 560 neurons; paired Student's t test). However, similar to layer 2/3 neurons, there was also a significant activation of layer 5 PT neurons even in the absence of a measurable

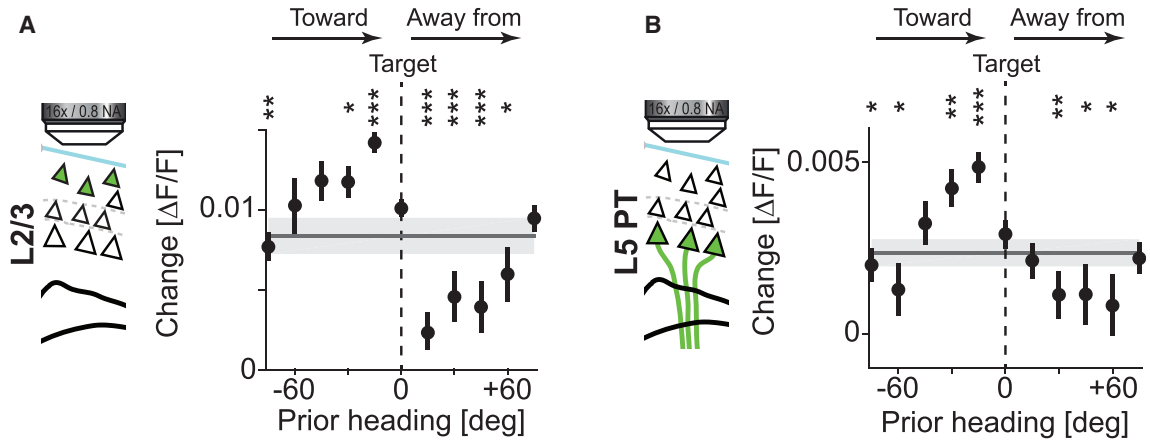

Figure 5. Activity during Spontaneous Turns Is Higher when the Turn Is Taken Toward the Target

(A) Average activity during spontaneous turns in layer 2/3 neurons as a function of the heading in a window −0.625 s to −0.125 s preceding the turn. Turns were acceleration matched (see STAR Methods and Figure S8) and binned such that a negative prior heading indicates a turn toward the target and a positive prior heading a turn away from the target. In this analysis, we included data from all training days (days 1 to 8). Error bars indicate SEM over turns. Horizontal gray line and shading is the average response and SEM over turns. *$p < 0.05$, **$p < 0.01$, ***$p < 10^{-3}$; Student's t test against the center bin. Bins that are not significant are not marked.

(B) As in (A), but for layer 5 PT neurons.

turning response (Figures 6C and 6F; first bin versus no response, layer 2/3: $p < 10^{-29}$; n = 1,154 neurons; layer 5 PT: $p < 10^{-11}$; n = 560 neurons; paired Student's t test). Thus, while the activation of layer 2/3 neurons to a visual offset perturbation was independent of subsequent behavioral response, the activation of layer 5 PT neurons remained predictive of the subsequent behavioral response.

Visual Offset Perturbations Activate Layer 2/3 Neurons Irrespective of Motor Response Direction

The fact that layer 2/3 neuron activation to perturbations occurred independently of the subsequent motor behavior could be the result of a concurrent activation of multiple possible motor plan encoding ensembles in response to an unexpected perturbation. If this were the case, we would expect both contra- and ipsiversive turn-responsive layer 2/3 neurons to be activated independent of the direction of the perturbation. We compared responses of contra- and ipsiversive turn neurons during spontaneous and induced turns, sorting neurons by their response magnitude during spontaneous contraversive turns (Figures 7A and 7G). During spontaneous turns, both layer 2/3 and layer 5 PT neurons tended to be activated only during either contra- or ipsiversive turns, but not both. The average response of contraversive neurons during spontaneous ipsiversive turns was a net decrease of mean activity and vice versa (Figures 7B and 7H). This decrease was likely the result of a response decay to the preceding contraversive turn. To quantify the similarity of the population response during spontaneous contraversive turns compared to the population response during spontaneous ipsiversive turns, we computed the correlation coefficient of the population vector of activity during ipsi- and contraversive turns as a function of time relative to the turn onset (Figures 7C and 7I). The population activity during contraversive turns in both layer 2/3 and layer 5 PT neurons was negatively correlated with the population activity during ipsiversive turns before and after turn onset. The negative correlation preceding the turn is likely a consequence of the fact that mice tend to execute contra- and ipsiversive turns in alternation.

To test whether the neurons that are activated during spontaneous turns are also activated during induced turns, we quantified the responses of the same neurons during induced turns. Neurons that responded during spontaneous contraversive turns also responded during induced contraversive turns (Figures 7D and 7J). Consistent with the idea that induced turns result in a concurrent activation of contra- and ipsiversive neurons, we found that contraversive neurons also exhibited an initial response during induced ipsiversive turns (Figures 7D–7E, 7J, and 7K). This initial response during induced turns in the non-preferred direction was more pronounced in layer 2/3 than in layer 5 PT neurons. Based on the layer 2/3 responses, we estimated the duration of this concurrent activation to be 666 ms ± 9 ms (mean ± SEM, n = 1,154 neurons, see STAR Methods). By analyzing the correlation of the population activity vectors during induced contraversive and induced ipsiversive turns, we found that the activity vectors were initially positively correlated only in layer 2/3 but not in layer 5 PT neurons (Figures 7F and 7L). Thus, immediately following an unexpected perturbation, both contra- and ipsiversive turn-responsive neurons are activated in layer 2/3, irrespective of their response preference during spontaneous turns. It is conceivable that the layer 2/3 activation in response to perturbations is not a co-activation of ipsi- and contraversive turn neurons, but a general response to any unexpected sensory stimulus. We therefore examined the responses to unexpected air puffs to the neck resulting in a startle response. We indeed found a response to air puffs in both layer 2/3 and layer 5 PT neurons, but the activity pattern elicited by the air puff did not correlate with that elicited by either ipsi- or contraversive visual offset perturbations (Figure S7),

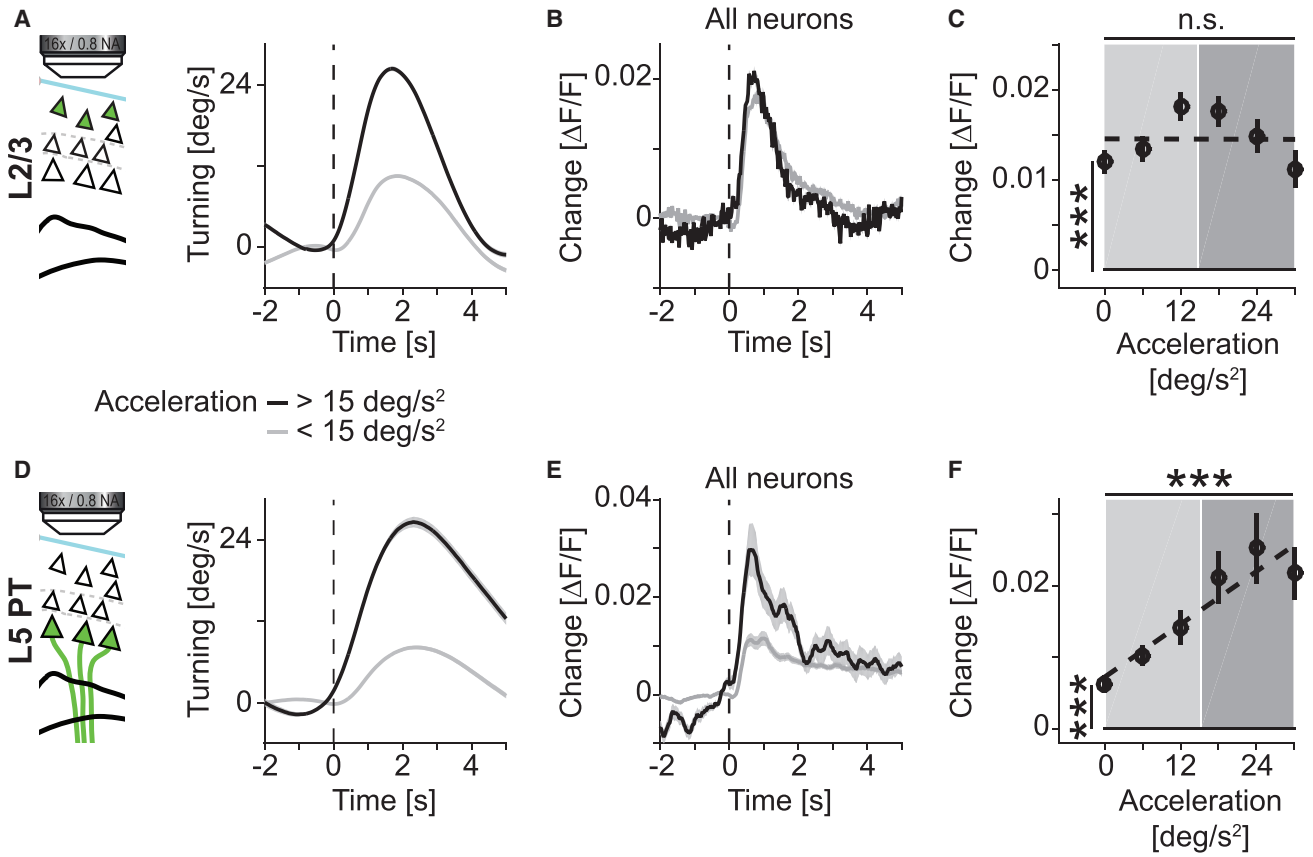

Figure 6. Visual Offset Perturbations Activate Layer 2/3 Neurons Independent of the Amplitude of the Induced Turn

(A) We split visual offset perturbation-induced turns recorded throughout training (days 3 to 8) into bins of high (black) and low (gray) accelerations. Shading indicates SEM over turns (number of turns for high acceleration bin: n = 402; low acceleration bin: n = 659).

(B) Average response in layer 2/3 neurons for the high (black line) and low (gray line) acceleration turns as defined in (A). Both low and high acceleration result in almost identical activation of layer 2/3 neurons (n = 1,154 neurons).

(C) Average population response of layer 2/3 neurons as a function of acceleration of the induced turn. Error bars indicate SEM over neurons (n = 1,154 neurons). Dashed black line is a linear fit to the data. Shading marks bins used for the turning and activity traces in (A) and (B). ***$p < 10^{-3}$, Student's t test of first bin versus no response; n.s.,: not significant, paired Student's t test of first versus last bin. We found no evidence of a linear trend ($p = 0.86$, $R^2 = 10^{-6}$, n = 1,154 neurons; linear trend analysis; see STAR Methods).

(D) As in (A), but for layer 5 PT experiments (number of turns for high acceleration bin: n = 966; low acceleration bin: n = 1,167).

(E) As in (B), but for layer 5 PT neurons (n = 560 neurons).

(F) As in (C), but for layer 5 PT neurons (n = 560 neurons). ***$p < 10^{-3}$; Student's t test of first bin versus no response. ***$p < 10^{-3}$; paired Student's t test of first versus last bin. Linear trend analysis (see STAR Methods) indicated a significant linear trend ($p < 10^{-7}$, $R^2 = 0.01$, n = 560 neurons).

demonstrating that motor cortex response patterns are specific to the applied sensory perturbation.

To test whether the positive correlation between population activity vector during contra- and ipsiversive turns was the result of a symmetric co-activation of both contra- and ipsiversive neurons, we projected the population activity vector onto the two-dimensional subspace spanned by the activity patterns during contra- and ipsiversive spontaneous turns as a function of time (see STAR Methods). We did this for every offset perturbation separately and computed average trajectories. Consistent with a symmetric co-activation of both contra- and ipsiversive turn activity patterns, the population activity in layer 2/3 after a visual offset perturbation initially follows a trajectory near the line of unity between the two population activity patterns for contra- and ipsiversive turns (Figure 8A). Consistent with the observation that in layer 5 PT neurons we found no evidence for a positive correlation of population activity during contra- and ipsiversive turns (Figure 7L), we also find no evidence for co-activation of activity patterns in layer 5 PT neurons (Figure 8B). One interpretation is that in layer 2/3, visual offset perturbations result in an initially symmetric co-activation of the motor response patterns of both contra- and an ipsiversive turns and that one of the two activity patterns is selected through sequential processing in motor cortex to eventually activate only one of the two in layer 5 PT neurons (Figure 8C). Based on this, one would expect layer 5 IT neurons that are in between the layer 2/3 and layer 5 PT neurons in this processing hierarchy to exhibit intermediate effects. Layer 5 IT neurons receive strong input from layer 2/3 neurons and have a mostly unidirectional projection onto layer 5 PT neurons (Anderson

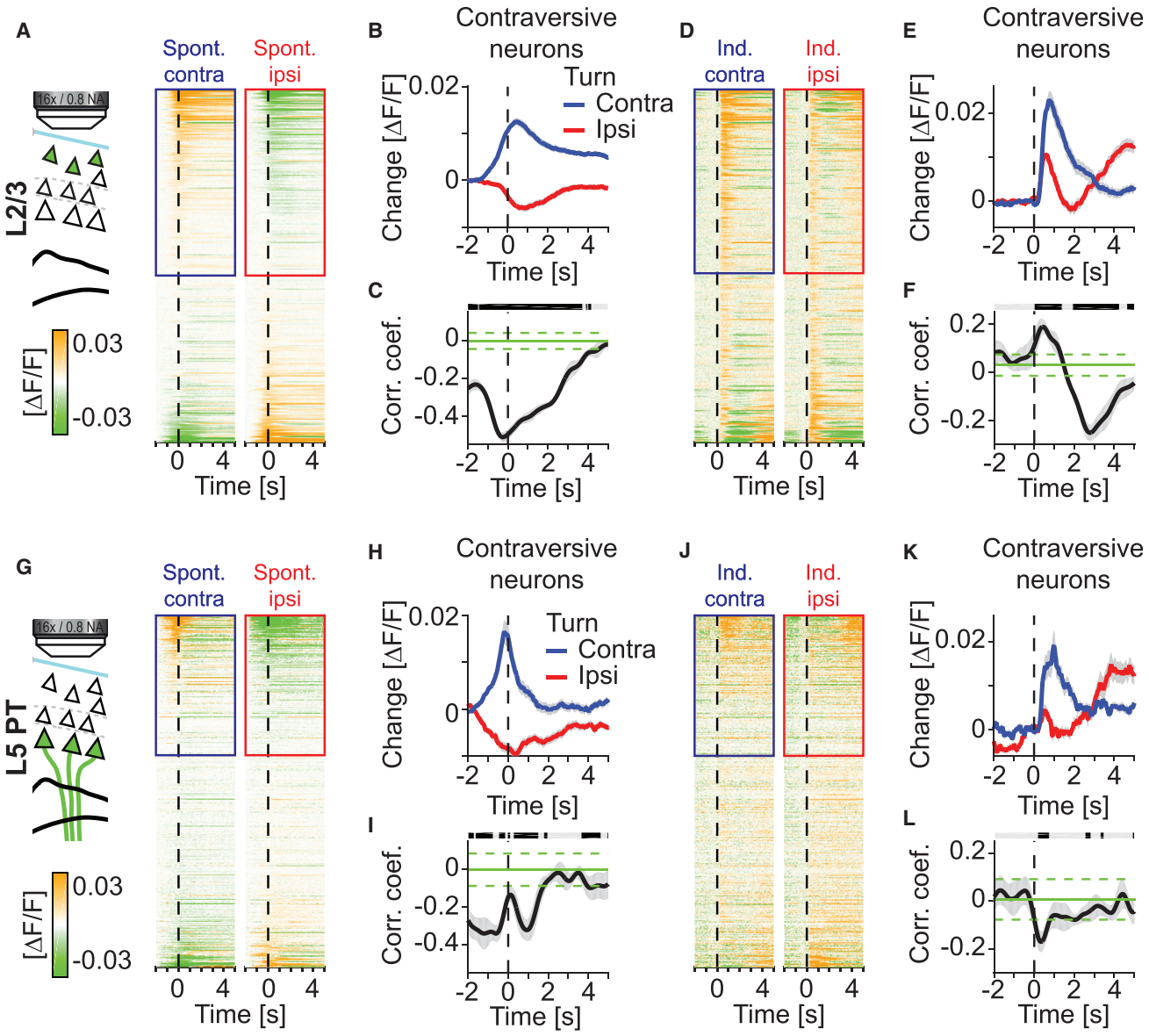

Figure 7. Spontaneous Turn-Responsive Cells Are Also Activated during Visual Offset Perturbation-Induced Turns

(A) Time course of average fluorescence of all layer 2/3 neurons (n = 1,154 neurons) during spontaneous contraversive (left) and ipsiversive (right) turns executed throughout training (days 1 to 8). Neurons are sorted by their selectivity during contraversive turns.

(B) Average neuronal activity of contraversive neurons (marked by blue and red box in A) during spontaneous contraversive (blue) and ipsiversive (red) turns. Shading indicates SEM over neurons (n = 616).

(C) Pearson's correlation coefficient of the population vector during contraversive and ipsiversive turns as a function of time around turn onset (black line, gray shading marks standard deviation over turns). Horizontal green lines mark mean (solid) and standard deviation (dashed) of random correlation. Horizontal black line marks time bins in which correlation is significantly different from chance (gray indicates bins that are not significant).

(D) Same as (A), but for visual offset perturbation-induced turns executed during training days 3 to 8. Sorting of neurons is the same as in (A).

(E) Same as (B), but for visual offset perturbation-induced turns executed during training days 3 to 8. Initially, contraversive neurons are activated during both contraversive and ipsiversive induced turns.

(F) Same as (C), but for visual offset perturbation-induced turns. Correlation of population vectors during induced turns is initially positive and only becomes negative approximately 2 s after onset of the visual offset perturbation.

(G) Same as (A), but for layer 5 PT neurons (n = 560 neurons).

(H) Same as (B), but for layer 5 PT neurons (n = 229 neurons, as selected in G).

(I) Same as (C), but for layer 5 PT neurons.

(J) Same as (D), but for layer 5 PT neurons.

(K) Same as (E), but for layer 5 PT neurons.

(L) Same as (F), but for layer 5 PT neurons. In contrast to layer 2/3, we find no evidence of a positive correlation of population vectors in layer 5 PT neurons.

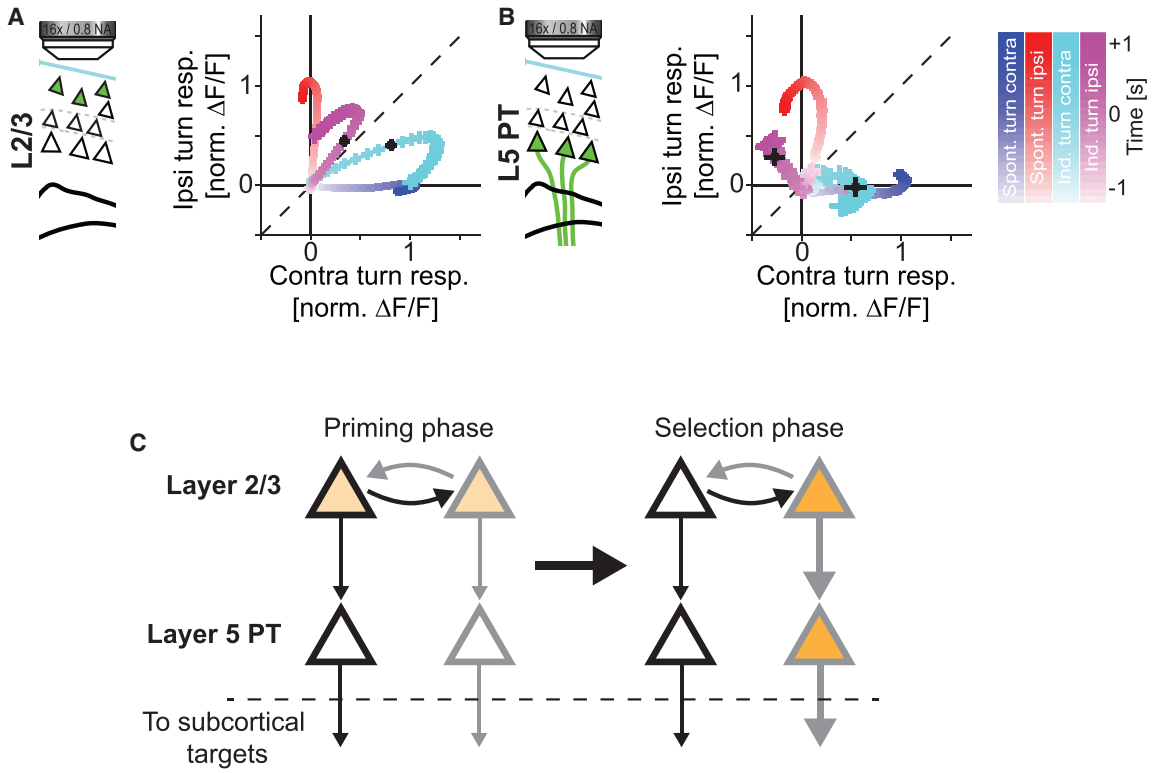

Figure 8. Activity Patterns for Spontaneous Contra- and Ipsiversive Turns Are Co-activated in Layer 2/3 during Visual Offset Perturbation-Induced Turns

(A) Projections of the population vector during spontaneous contraversive (blue) and spontaneous ipsiversive (red) executed throughout training (days 1 to 8) onto the plane spanned by the population vector 1 s after turn onset during spontaneous contraversive and spontaneous ipsiversive turns. Origin of the coordinate system is the mean population vector preceding turns. Shading of the maker indicates time relative to turn onset. We then projected the population activity vector during induced contraversive (cyan) and induced ipsiversive turns (magenta) executed during training days 3 to 8 onto the same coordinate system. Black crosses mark the first bin with the first significant change in turning velocity following visual offset perturbation. Error bars indicate SEM over turns. Dashed black line marks line of unity.

(B) As in (A), but for layer 5 PT responses.

(C) Model for the response of motor cortex to unexpected feedback perturbations. In an initial phase of the response, multiple assemblies of neurons, the activity of which we speculate corresponds to different motor plans, are co-activated and primed in layer 2/3. These assemblies could be separately driven by sensory evidence, and potentially directly compete. At a later time, during the movement selection phase of the response, the dominant activation pattern of layer 2/3 can recruit the corresponding assembly in layer 5 that then drives a behavioral response by activating subcortical motor control centers.

et al., 2010; Kiritani et al., 2012). We recorded the activity of layer 5 IT neurons in *Tlx3-Cre(PL56)* mice throughout training and found that the responses of layer 5 IT neurons during spontaneous turns were similar to those in layer 2/3 and layer 5 PT neurons (Figures S8A–S8E). However, the learning-related changes in layer 5 IT neurons were intermediate between those observed in the other two neuron types (Figure S8F). Similar to the responses in layer 2/3, activation of layer 5 IT neurons during induced turns exhibited no linear increase with increasing acceleration of the subsequent turn (Figures S8G–S8I). However, even though the correlation of population vector activity during ipsi- and contraversive-induced turns was positive just above chance, we found no evidence of a symmetric co-activation of contra- and ipsiversive neurons during induced turns (Figures S8J–S8L). Thus, these data are consistent with a model in which layer 2/3, layer 5 IT, and layer 5 PT form a sequential processing hierarchy that selects an appropriate motor output in response to a sensory perturbation.

DISCUSSION

The precise role of motor cortex in the control of movement is still unclear. Here, we demonstrate that inactivation or lesions of motor cortex interfere with the mouse's ability to learn and execute a virtual navigation task, despite the fact that the ability to execute the movements necessary to complete the task remained virtually unimpaired. These results are consistent with the interpretation that the impairment in task learning and execution results from an inability of the mouse to execute movements under visual guidance but not movements per se. Recording neural activity during unexpected visual offset perturbations, we found that responses in layer 2/3 to unexpected visual feedback are driven by the visual offset and do not correlate with the magnitude of the resulting behavioral correction. Moreover, the neuronal response to a visual offset perturbation initially is a co-activation of both ipsi- and contraversive neurons. In contrast, responses in layer 5 PT neurons maintain the linear

relationship with the magnitude of the induced turn that they show during spontaneous turns, without co-activation of ipsi- and contraversive neurons. We discuss our findings in the context of specific requirements of motor cortical signaling during sensory guided behavior, the specificity of cortical response patterns during these behaviors, as well as the influence of learning on motor cortical ensemble activity.

The Involvement of Motor Cortex in the Control of Movement

Cortex evolved to complement a functional sub-cortical motor control system. It exerts its influence on movement through interactions with neuronal circuits distributed throughout the central nervous system. While neuronal circuits in the spinal cord are essential to produce and support basic movement patterns including alternation of left-right and extension-flexion phases during locomotion (Kiehn, 2016), neurons in the brainstem with descending projections to the spinal cord are key in instructing movement execution in different species (Esposito et al., 2014; Jankowska and Edgley, 2006; Lawrence and Kuypers, 1968). Brainstem nuclei in turn are targets of major descending projections from cortical as well as subcortical motor areas (Jankowska and Edgley, 2006; Kably and Drew, 1998; Kuypers and Lawrence, 1967). The effect of lesion or inactivation of motor cortex is highly species dependent, consistent with a role of motor cortex that, during evolution, initially may have been merely modulatory. Cortical control of movement may therefore have co-evolved with an increasing reliance of species on cortical processing of sensory input providing the necessary information to guide movement with accuracy and precision, especially when the extraction of sensory information requires complex processing. In agreement with such a model, effects of motor cortex lesion in rodents are most pronounced when the task requires fine digit control (Whishaw et al., 1998), when animals encounter novel sensory conditions and movement coordination requires rapid sensory feedback control (Lopes et al., 2016), or when animals are still in the process of learning to control the movement (Kawai et al., 2015). It is thus conceivable that motor cortex functions to structure and adjust movements based on incoming sensory information processed in cortex.

To test this model, we developed a virtual navigation task for mice that requires visually guided control of movement. We found that inhibition of motor cortex impairs the ability of the mouse to execute turns induced by unexpected visual offsets (Figure 2). Inhibition of motor cortex also impaired the ability of the mouse to perform the task, but did not prevent the mouse from executing spontaneous turns. Considering that spontaneous turns can be executed either with or without visual guidance, and that visually guided spontaneous turns are necessary to perform the task, our findings suggest that motor cortex is necessary for the visual guidance of turns. Based on this, we would expect to find higher activity in M1 during visually guided spontaneous turns than during non-visually guided spontaneous turns. For any individual spontaneous turn, we cannot determine whether it was executed under visual guidance or non-visually guided. However, given that mice are trained to navigate to a visual target, we can assume that visually guided spontaneous turns are directed toward the target, while non-visually guided turns are equally likely to occur toward or away from the target. To test whether there is a difference in activity between visually guided and non-visually guided spontaneous turns, we split turns into those directed toward the target (which are a combination of both visually guided and non-visually guided turns) and those directed away from the target (which are non-visually guided turns). Interestingly, we observed that activation in motor cortical neurons was significantly higher for target-directed spontaneous turns than for turns directed away from the target (Figure 5). Thus, while motor cortex clearly possesses the capacity to drive movements when stimulated (Harrison et al., 2012; Tennant et al., 2011), our results suggest that in this virtual navigation task motor cortical control is exerted mainly during visually guided behavior. These results are consistent with the results of experiments performed in cats, which showed that motor cortical neurons are strongly activated when cats step over an obstacle placed in front of them but not in the preceding period walking on a runway (Drew et al., 2002). In this context, cortical circuits for visually guided control of locomotion have been suggested to involve the parietal cortex (Drew and Marigold, 2015), an area that is directly connected with visual cortex in rodents (Kolb and Walkey, 1987). These inputs could provide motor cortex with the signals necessary to perform visually guided behavior, similar to inputs from somatosensory cortex that are necessary for somatosensory control of movement (Mathis et al., 2017; Sreenivasan et al., 2016).

Differential Roles of Layer 2/3 and Layer 5 in Response to Unexpected Feedback Perturbations

Motor cortex activity has been shown to correlate with a variety of movement parameters in mice (Dombeck et al., 2009; Komiyama et al., 2010; Li et al., 2015; Peters et al., 2017) and primates (Churchland et al., 2012; Moran and Schwartz, 1999; Townsend et al., 2006). Consistent with a correlation between neuronal activity in motor cortex and specific movement parameters, we found that neuronal activity in both layer 2/3 and layer 5 PT neurons exhibited a linear increase with increasing acceleration of spontaneous turns (Figure 3) and most neurons were selectively activated during either ipsi- or contraversive turns (Figure 7). Interestingly, we found that a similar linear increase in neuronal activity was not apparent for running onset activity as a function of forward running onset acceleration in our task (Figure S4). It is possible that the acceleration at running onsets is not dependent on visual control and hence is not influenced by motor cortex. Consistent with such a model, mice were still able to initiate running during optogenetic inhibition of motor cortex, and recent work also suggests that short-latency motor cortex signaling is not needed during walking (Miri et al., 2017). Motor cortex might generally retain a linear relationship between neuronal activity and movement amplitude along coding dimensions during spontaneous movement initiation. Neuronal activity in motor cortex has been shown to be tuned not just to the activation of a muscle, but to the context in which this activation occurs (Griffin et al., 2015), and whether the activation was in response to an unexpected perturbation (Stout et al., 2015). Consistent with a central role of motor cortex in the detection of and the response to unexpected sensory perturbations, we

found that layer 2/3 and layer 5 PT neurons were differentially activated in response to unexpected feedback perturbations: initial activation of layer 2/3 neurons did not depend on either acceleration or direction of the subsequent induced turn, while layer 5 PT neurons retained both a linear dependence on turning acceleration and the selectivity for turn direction they exhibited during spontaneous behavior (Figure 6). Combining this with the finding that motor cortex is necessary for turn initiation in response to an unexpected feedback perturbation but not for the execution of spontaneous turns per se, these data may point to a role of motor cortex in the response to unexpected sensory perturbations (Adams et al., 2013). Our data would be consistent with a model in which layer 2/3 neurons signal a deviation between intended and actual motor state that updates an internal representation of the intended motor state in layer 5 PT neurons. Such a description would be computationally equivalent to a predictive processing description of visual cortex, where layer 2/3 neurons have been postulated to signal deviations between actual and expected visual input that function to update an internal representation of the visual scene in layer 5 neurons (Attinger et al., 2017; Fiser et al., 2016; Rao and Ballard, 1999; Zmarz and Keller, 2016).

Alternatively, the concurrent activation of ipsi- and contraversive layer 2/3 neurons in response to unexpected sensory perturbations would also be consistent with a model in which layer 2/3 concurrently activates both ipsi- and contraversive turn motor plan ensembles. In this model, either the ipsi- or contraversive ensemble in layer 5 PT is then selected for output to subcortical structures, likely as a consequence of input from other cortical areas and local cortical processing. This would be consistent with the finding that in primate motor cortex, different movement goals can be simultaneously represented during movement preparation (Klaes et al., 2011). A sequential selection process is also supported by the known hierarchical local connectivity in motor cortex between layer 2/3, layer 5 IT, and layer 5 PT, which is predominantly unidirectional (Anderson et al., 2010; Kiritani et al., 2012; Weiler et al., 2008), and the observation that responses in layer 5 IT neurons were intermediate between the ones we observed in layer 2/3 and layer 5 PT (Figure S8). Neither of these models likely exhaustively describes the function of motor cortex, but they both point to a common computational goal of motor cortex: increasing the accuracy and efficiency with which an animal can react to a sensory perturbation.

Learning-Related Activation Changes Could Reflect Changes in the Precision of Sensorimotor Control

Motor learning is typically accompanied by functional and structural plasticity in motor cortex (Huber et al., 2012; Komiyama et al., 2010; Ma et al., 2016; Masamizu et al., 2014; Peters et al., 2017; Yang et al., 2009). Consistent with this, we observed systematic changes in activation during spontaneous turns in both layer 2/3 and layer 5 PT neurons with increasing task performance over days (Figure 4). Also consistent with previous findings, activation of both layer 2/3 and layer 5 PT neurons was initially stronger during contraversive turns than during ipsiversive turns (Cui et al., 2013; Li et al., 2015). Interestingly, with experience, activation of layer 2/3 during contraversive turns decreased to the level of activation during ipsiversive turns, whereas in layer 5 PT neurons, the activity during contraversive turns was larger than during ipsiversive turns and increased further with experience. Note that we do not know whether these changes we observe in motor cortex with learning are merely a consequence of a change in behavioral strategy or are the cause of that change. As task performance increases, the frequency and magnitude of deviations from intended trajectory should decrease while the vigor and precision with which corrective movements are executed should increase. Thus, as mice gain experience traversing the virtual tunnel, the movement error, which is necessary for trial-to-trial motor adaptations (Inoue et al., 2016), is systematically reduced. We indeed found evidence for systematic motor adaptations in the way mice learn to correct their movement trajectory: with training, the fraction of turns directed toward the target increased (Figure S6). Additionally, we found that the stability of responses in layer 5 PT neurons increased over the course of learning and is higher than that of layer 2/3 neurons (Figure S5). This is consistent with movement error detection in layer 2/3 that drives movement adaptation and hence does not stabilize with learning, while activity in layer 5 PT neurons that mediate motor output stabilizes with increasing behavioral stereotypy in a given task.

Conclusion

In summary, we propose that motor cortex influences motor behavior under conditions in which movement is guided by unexpected sensory input. The mechanism by which motor cortex exerts influence on movement control might be by the activation of different possible motor plan ensembles in layer 2/3 neurons in response to deviations from expected sensory input. Of these plans, one is selected for execution by the activation of an appropriate subset of layer 5 PT neurons. Such a model would also explain why the dependence on motor cortex for motor behavior parallels the species' reliance on cortex for sensory processing.

STAR★METHODS

Detailed methods are provided in the online version of this paper and include the following:

- KEY RESOURCES TABLE
- CONTACT FOR REAGENT AND RESOURCE SHARING
- EXPERIMENTAL MODEL AND SUBJECT DETAILS
  - Animals and surgery
- METHOD DETAILS
  - Surgery and virus injections
  - Virtual reality setup and behavioral paradigm
  - Optogenetic inhibition experiments
  - Two-photon calcium imaging
  - Histology
- QUANTIFICATION AND STATISTICAL ANALYSIS
  - Data analysis
  - Behavioral data analyses
  - Calcium imaging data analyses
- DATA AND SOFTWARE AVAILABILITY

SUPPLEMENTAL INFORMATION

Supplemental Information includes eight figures, two tables, and two movies and can be found with this article online at https://doi.org/10.1016/j.neuron.2018.07.046.

ACKNOWLEDGMENTS

We thank Bence Ölveczky for comments on an earlier version of the manuscript. We thank Daniela Gerosa-Erni for production of the AAV vectors and Marcus Leinweber for help with the construction of the microscope and virtual reality setup, and the members of the Arber and the Keller labs for discussion and support. M.H. and S.A. were supported by ERC Advanced Grant No 692617, Kanton Basel-Stadt, and the Louis Jeantet Prize for Medicine, and all authors were supported by the Swiss National Science Foundation and the Novartis Research Foundation.

AUTHOR CONTRIBUTIONS

M.H. performed the experiments and analyzed the data. M.H., S.A., and G.B.K. designed the experiments and wrote the manuscript.

DECLARATION OF INTERESTS

The authors declare no competing interests.

Received: December 11, 2017
Revised: June 6, 2018
Accepted: July 25, 2018
Published: August 23, 2018

REFERENCES

Adams, R.A., Shipp, S., and Friston, K.J. (2013). Predictions not commands: active inference in the motor system. Brain Struct. Funct. *218*, 611–643.

Anderson, C.T., Sheets, P.L., Kiritani, T., and Shepherd, G.M.G. (2010). Sublayer-specific microcircuits of corticospinal and corticostriatal neurons in motor cortex. Nat. Neurosci. *13*, 739–744.

Armstrong, D.M., and Drew, T. (1984). Discharges of pyramidal tract and other motor cortical neurones during locomotion in the cat. J. Physiol. *346*, 471–495.

Attinger, A., Wang, B., and Keller, G.B. (2017). Visuomotor Coupling Shapes the Functional Development of Mouse Visual Cortex. Cell *169*, 1291–1302.e14.

Beloozerova, I.N., and Sirota, M.G. (1993a). The role of the motor cortex in the control of vigour of locomotor movements in the cat. J. Physiol. *461*, 27–46.

Beloozerova, I.N., and Sirota, M.G. (1993b). The role of the motor cortex in the control of accuracy of locomotor movements in the cat. J. Physiol. *461*, 1–25.

Beloozerova, I.N., Farrell, B.J., Sirota, M.G., and Prilutsky, B.I. (2010). Differences in movement mechanics, electromyographic, and motor cortex activity between accurate and nonaccurate stepping. J. Neurophysiol. *103*, 2285–2300.

Brecht, M., Schneider, M., Sakmann, B., and Margrie, T.W. (2004). Whisker movements evoked by stimulation of single pyramidal cells in rat motor cortex. Nature *427*, 704–710.

Chen, T.-W., Wardill, T.J., Sun, Y., Pulver, S.R., Renninger, S.L., Baohan, A., Schreiter, E.R., Kerr, R.A., Orger, M.B., Jayaraman, V., et al. (2013). Ultrasensitive fluorescent proteins for imaging neuronal activity. Nature *499*, 295–300.

Churchland, M.M., Cunningham, J.P., Kaufman, M.T., Foster, J.D., Nuyujukian, P., Ryu, S.I., and Shenoy, K.V. (2012). Neural population dynamics during reaching. Nature *487*, 51–56.

Cui, G., Jun, S.B., Jin, X., Pham, M.D., Vogel, S.S., Lovinger, D.M., and Costa, R.M. (2013). Concurrent activation of striatal direct and indirect pathways during action initiation. Nature *494*, 238–242.

Dombeck, D.A., Graziano, M.S., and Tank, D.W. (2009). Functional clustering of neurons in motor cortex determined by cellular resolution imaging in awake behaving mice. J. Neurosci. *29*, 13751–13760.

Drew, T., and Marigold, D.S. (2015). Taking the next step: cortical contributions to the control of locomotion. Curr. Opin. Neurobiol. *33*, 25–33.

Drew, T., Jiang, W., and Widajewicz, W. (2002). Contributions of the motor cortex to the control of the hindlimbs during locomotion in the cat. Brain Res. Brain Res. Rev. *40*, 178–191.

Esposito, M.S., Capelli, P., and Arber, S. (2014). Brainstem nucleus MdV mediates skilled forelimb motor tasks. Nature *508*, 351–356.

Farrell, B.J., Bulgakova, M.A., Sirota, M.G., Prilutsky, B.I., and Beloozerova, I.N. (2015). Accurate stepping on a narrow path: mechanics, EMG, and motor cortex activity in the cat. J. Neurophysiol. *114*, 2682–2702.

Ferrier, D. (1874). Experiments on the Brain of Monkeys. Proc. R. Soc. Lond. *23*, 409–430.

Fiser, A., Mahringer, D., Oyibo, H.K., Petersen, A.V., Leinweber, M., and Keller, G.B. (2016). Experience-dependent spatial expectations in mouse visual cortex. Nat. Neurosci. *19*, 1658–1664.

Georgopoulos, A.P., Schwartz, A.B., and Kettner, R.E. (1986). Neuronal population coding of movement direction. Science *233*, 1416–1419.

Gerfen, C.R., Paletzki, R., and Heintz, N. (2013). GENSAT BAC cre-recombinase driver lines to study the functional organization of cerebral cortical and basal ganglia circuits. Neuron *80*, 1368–1383.

Griffin, D.M., Hoffman, D.S., and Strick, P.L. (2015). Corticomotoneuronal cells are "functionally tuned". Science *350*, 667–670.

Guo, Z.V., Li, N., Huber, D., Ophir, E., Gutnisky, D., Ting, J.T., Feng, G., and Svoboda, K. (2014). Flow of cortical activity underlying a tactile decision in mice. Neuron *81*, 179–194.

Harrison, T.C., Ayling, O.G.S., and Murphy, T.H. (2012). Distinct cortical circuit mechanisms for complex forelimb movement and motor map topography. Neuron *74*, 397–409.

Huber, D., Gutnisky, D.A., Peron, S., O'Connor, D.H., Wiegert, J.S., Tian, L., Oertner, T.G., Looger, L.L., and Svoboda, K. (2012). Multiple dynamic representations in the motor cortex during sensorimotor learning. Nature *484*, 473–478.

Inoue, M., Uchimura, M., and Kitazawa, S. (2016). Error Signals in Motor Cortices Drive Adaptation in Article Error Signals in Motor Cortices Drive Adaptation in Reaching. Neuron *90*, 1114–1126.

Jankowska, E., and Edgley, S.A. (2006). How can corticospinal tract neurons contribute to ipsilateral movements? A question with implications for recovery of motor functions. Neuroscientist *12*, 67–79.

Kably, B., and Drew, T. (1998). Corticoreticular pathways in the cat. I. Projection patterns and collaterization. J. Neurophysiol. *80*, 389–405.

Kawai, R., Markman, T., Poddar, R., Ko, R., Fantana, A.L., Dhawale, A.K., Kampff, A.R., and Ölveczky, B.P. (2015). Motor cortex is required for learning but not for executing a motor skill. Neuron *86*, 800–812.

Kiehn, O. (2016). Decoding the organization of spinal circuits that control locomotion. Nat. Rev. Neurosci. *17*, 224–238.

Kiritani, T., Wickersham, I.R., Seung, H.S., and Shepherd, G.M.G. (2012). Hierarchical connectivity and connection-specific dynamics in the corticospinal-corticostriatal microcircuit in mouse motor cortex. J. Neurosci. *32*, 4992–5001.

Kita, T., and Kita, H. (2012). The subthalamic nucleus is one of multiple innervation sites for long-range corticofugal axons: a single-axon tracing study in the rat. J. Neurosci. *32*, 5990–5999.

Klaes, C., Westendorff, S., Chakrabarti, S., and Gail, A. (2011). Choosing goals, not rules: deciding among rule-based action plans. Neuron *70*, 536–548.

Kolb, B., and Walkey, J. (1987). Behavioural and anatomical studies of the posterior parietal cortex in the rat. Behav. Brain Res. *23*, 127–145.

Komiyama, T., Sato, T.R., O'Connor, D.H., Zhang, Y.-X., Huber, D., Hooks, B.M., Gabitto, M., and Svoboda, K. (2010). Learning-related fine-scale

specificity imaged in motor cortex circuits of behaving mice. Nature *464*, 1182–1186.

Kuypers, H.G., and Lawrence, D.G. (1967). Cortical projections to the red nucleus and the brain stem in the Rhesus monkey. Brain Res. *4*, 151–188.

Lang, C.E., and Schieber, M.H. (2003). Differential impairment of individuated finger movements in humans after damage to the motor cortex or the corticospinal tract. J. Neurophysiol. *90*, 1160–1170.

Lawrence, D.G., and Kuypers, H.G. (1968). The functional organization of the motor system in the monkey. II. The effects of lesions of the descending brain-stem pathways. Brain *91*, 15–36.

Leinweber, M., Ward, D.R., Sobczak, J.M., Attinger, A., and Keller, G.B. (2017). A Sensorimotor Circuit in Mouse Cortex for Visual Flow Predictions. Neuron *96*, 1204.

Li, N., Chen, T.W., Guo, Z.V., Gerfen, C.R., and Svoboda, K. (2015). A motor cortex circuit for motor planning and movement. Nature *519*, 51–56.

Lopes, G., Nogueira, J., Paton, J.J., and Kampff, A.R. (2016). A robust role for motor cortex. bioRxiv. https://doi.org/10.1101/058917.

Ma, L., Qiao, Q., Tsai, J.-W., Yang, G., Li, W., and Gan, W.-B. (2016). Experience-dependent plasticity of dendritic spines of layer 2/3 pyramidal neurons in the mouse cortex. Dev. Neurobiol. *76*, 277–286.

Madisen, L., Zwingman, T.A., Sunkin, S.M., Oh, S.W., Zariwala, H.A., Gu, H., Ng, L.L., Palmiter, R.D., Hawrylycz, M.J., Jones, A.R., et al. (2010). A robust and high-throughput Cre reporting and characterization system for the whole mouse brain. Nat. Neurosci. *13*, 133–140.

Marple-Horvat, D.E., Amos, A.J., Armstrong, D.M., and Criado, J.M. (1993). Changes in the discharge patterns of cat motor cortex neurones during unexpected perturbations of on-going locomotion. J. Physiol. *462*, 87–113.

Masamizu, Y., Tanaka, Y.R., Tanaka, Y.H., Hira, R., Ohkubo, F., Kitamura, K., Isomura, Y., Okada, T., and Matsuzaki, M. (2014). Two distinct layer-specific dynamics of cortical ensembles during learning of a motor task. Nat. Neurosci. *17*, 987–994.

Mathis, M.W., Mathis, A., and Uchida, N. (2017). Somatosensory Cortex Plays an Essential Role in Forelimb Motor Adaptation in Mice. Neuron *93*, 1493–1503.e6.

Miri, A., Warriner, C.L., Seely, J.S., Elsayed, G.F., Cunningham, J.P., Churchland, M.M., and Jessell, T.M. (2017). Behaviorally Selective Engagement of Short-Latency Effector Pathways by Motor Cortex. Neuron *95*, 683–696.e11.

Moran, D.W., and Schwartz, A.B. (1999). Motor cortical representation of speed and direction during reaching. J. Neurophysiol. *82*, 2676–2692.

Morishima, M., and Kawaguchi, Y. (2006). Recurrent connection patterns of corticostriatal pyramidal cells in frontal cortex. J. Neurosci. *26*, 4394–4405.

Murata, Y., Higo, N., Oishi, T., Yamashita, A., Matsuda, K., Hayashi, M., and Yamane, S. (2008). Effects of motor training on the recovery of manual dexterity after primary motor cortex lesion in macaque monkeys. J. Neurophysiol. *99*, 773–786.

Peters, A.J., Lee, J., Hedrick, N.G., O'Neil, K., and Komiyama, T. (2017). Reorganization of corticospinal output during motor learning. Nat. Neurosci. *20*, 1133–1141.

Rao, R.P.N., and Ballard, D.H. (1999). Predictive coding in the visual cortex: a functional interpretation of some extra-classical receptive-field effects. Nat. Neurosci. *2*, 79–87.

Sreenivasan, V., Esmaeili, V., Kiritani, T., Galan, K., Crochet, S., and Petersen, C.C.H. (2016). Movement Initiation Signals in Mouse Whisker Motor Cortex. Neuron *92*, 1368–1382.

Stout, E.E., Sirota, M.G., and Beloozerova, I.N. (2015). Known and unexpected constraints evoke different kinematic, muscle, and motor cortical neuron responses during locomotion. Eur. J. Neurosci. *42*, 2666–2677.

Tennant, K.A., Adkins, D.L., Donlan, N.A., Asay, A.L., Thomas, N., Kleim, J.A., and Jones, T.A. (2011). The organization of the forelimb representation of the C57BL/6 mouse motor cortex as defined by intracortical microstimulation and cytoarchitecture. Cereb. Cortex *21*, 865–876.

Townsend, B.R., Paninski, L., and Lemon, R.N. (2006). Linear encoding of muscle activity in primary motor cortex and cerebellum. J. Neurophysiol. *96*, 2578–2592.

Vong, L., Ye, C., Yang, Z., Choi, B., Chua, S., Jr., and Lowell, B.B. (2011). Leptin action on GABAergic neurons prevents obesity and reduces inhibitory tone to POMC neurons. Neuron *71*, 142–154.

Weiler, N., Wood, L., Yu, J., Solla, S.A., and Shepherd, G.M.G. (2008). Top-down laminar organization of the excitatory network in motor cortex. Nat. Neurosci. *11*, 360–366.

Whishaw, I.Q., Gorny, B., and Sarna, J. (1998). Paw and limb use in skilled and spontaneous reaching after pyramidal tract, red nucleus and combined lesions in the rat: behavioral and anatomical dissociations. Behav. Brain Res. *93*, 167–183.

Yang, G., Pan, F., and Gan, W.-B. (2009). Stably maintained dendritic spines are associated with lifelong memories. Nature *462*, 920–924.

Zaaimi, B., Edgley, S.A., Soteropoulos, D.S., and Baker, S.N. (2012). Changes in descending motor pathway connectivity after corticospinal tract lesion in macaque monkey. Brain *135*, 2277–2289.

Zmarz, P., and Keller, G.B. (2016). Mismatch Receptive Fields in Mouse Visual Cortex. Neuron *92*, 766–772.

STAR★METHODS

KEY RESOURCES TABLE

REAGENT or RESOURCE	SOURCE	IDENTIFIER
Antibodies		
Chicken Anti-GFP	ThermoFisher	RRID: AB_2534023
Anti-NeuN	Millipore	RRID: AB_2298772
Alexa Fluor 488 Donkey Anti-Chicken IgY	Jackson ImmunoResearch	RRID: AB_2340375
Alexa Fluor 568 donkey anti - rabbit IgG	ThermoFisher	RRID: AB_2534017
Alexa Fluor 647 donkey anti - mouse IgG	ThermoFisher	RRID: AB_162542
Bacterial and Virus Strains		
AAV2/1-EF1a-GCaMP6f-WPRE	FMI Vector Core	N/A
AAV2/1-EF1a-DiO-GCaMP6f-WPRE	FMI Vector Core	N/A
Chemicals, Peptides, and Recombinant Proteins		
Isoflurane (Attane)	Provet	CAS 26221-73-3
Fentanyl	Actavis	CAS 990-73-8
Midazolam (Dormicum)	Roche	CAS 59467-96-8
Medetomidine (Dormitor)	Orion	CAS 86347-14-0
Flumazenil (Anexate)	Roche	CAS 78755-81-4
Atipamezole (Antisedan)	Orion Pharma	CAS 104054-27-5
Histoacryl	B. Braun	CAS 6606-65-1
Dental cement (Paladur)	Heraeus Kulzer	CAS 9066-86-8
Ibotenic acid	Sigma	CAS 2552-55-8
Experimental Models: Organisms/Strains		
Mouse: C57BL6/J	Charles River Laboratories	N/A
Mouse: Tg(Tlx3-Cre)PL58Gsat	MMRRC	RRID: MMRRC_036670-UCD
Mouse: Tg(Sim1-Cre)KJ18Gsat	Gerfen et al., 2013	RRID: MMRRC_031742-UCD
Mouse: Slc32a1$^{tm2(cre)Lowl}$/J	Vong et al., 2011	RRID: IMSR_JAX:016962
Mouse: B6.Cg-Gt(ROSA)26Sor$^{tm14(CAG-tdTomato)Hze}$/J	Madisen et al., 2010	RRID: IMSR_JAX:007914
Mouse: B6.Cg-Tg(Slc32a1-COP4*H134R/EYFP)8Gfng/J	The Jackson Laboratory	RRID: IMSR_JAX:014548
Software and Algorithms		
LabVIEW	National Instruments	RRID: SCR_014325
Iris: 2 photon scanning software	N/A	https://sourceforge.net/projects/iris-scanning/
MATLAB	The MathWorks	RRID: SCR_001622
Calliope: Image processing software	N/A	https://svn.code.sf.net/p/iris-scanning/calliope/
Other		
Titanium Headplate	Leinweber et al., 2017	Custom
Virtual reality setup	Leinweber et al., 2017	Custom

CONTACT FOR REAGENT AND RESOURCE SHARING

Further information and requests for resources and reagents should be directed to and will be fulfilled by the Lead Contact, Georg Keller (georg.keller@fmi.ch).

EXPERIMENTAL MODEL AND SUBJECT DETAILS

Animals and surgery

All animal procedures were approved by and carried out in accordance with guidelines of the Veterinary Department of the Canton Basel-Stadt, Switzerland. The mice used in this study were kept on a C57BL/6 background and were of the following genotype: 8

vGAT-Cre (Vong et al., 2011, RRID: IMSR_JAX:016962) x *ROSA-LSL-tdTom* (Madisen et al., 2010, RRID: IMSR_JAX:007914) mice were used for imaging layer 2/3 excitatory neurons, 11 *Sim1-Cre(KJ18)* mice for imaging layer 5 pyramidal tract (PT) neurons (Gerfen et al., 2013, RRID: MMRRC_031742-UCD), 9 *Tlx3-Cre(PL56)* (Gerfen et al., 2013, RRID: MMRRC_036670-UCD) were used for imaging layer 5 intratelencephalic (IT) projection neurons, 15 *vGAT::ChR2(H134R)-EYFP* (RRID: IMSR_JAX:014548) mice were used for optogenetic inhibition experiments, 5 *C57BL/6* were used for ibotenic acid lesion experiments, and 6 *C57BL/6* mice were used in optogenetic control experiments. Mice were group housed in a vivarium (light/dark cycle: 12/12 hr) and were 6 – 14 weeks old at the beginning of experiments. Experimental mice used were of both sexes.

METHOD DETAILS

Surgery and virus injections

For all surgical procedures, mice were anesthetized using a mixture of Fentanyl (0.05 mg/kg; Actavis), Midazolam (5.0 mg/kg; Dormicum, Roche) and Medetomidine (0.5 mg/kg; Domitor, Orion). In surgeries preparing for two-photon imaging experiments, a craniotomy of approximately 4 mm diameter was made over the right motor cortex centered on a location 0.5 mm anterior and 1.5 mm lateral of bregma. This corresponds approximately to the caudal forelimb area mapped by intracortical microstimulation (Tennant et al., 2011). We placed 5 to 9 injections of approximately 150 nL each of either unconditional AAV2/1-Ef1α-GCaMP6f (titer 10^{11} – 10^{12} GC/mL) for imaging layer 2/3 neurons or conditional AAV2/1-Ef1α-DIO-GCaMP6f (titer 10^{11} – 10^{12} GC/mL) for imaging layer 5 PT neurons within a radius of approximately 500 μm of the center of the target region. For ibotenic acid (5 g/L; Sigma) lesions, a single point injection of approximately 250 nL was made centered in the caudal forelimb area (CFA, 0.5 mm anterior and 1.5 mm lateral from bregma). For optogenetic experiments, the craniotomy was made to span motor cortex bilaterally. A circular 4 mm (imaging) or a custom-cut (optogenetics) coverslip was implanted with superglue (Pattex) to close the craniotomy. A custom-machined titanium head bar was attached to the skull using dental cement (Paladur, Heraeus). Anesthesia was antagonized by an intraperitoneal injection of a mixture of Flumazenil (0.5 mg/kg; Anexate, Roche) and Atipamezole (2.5 mg/kg; Antisedan, Orion Pharma) and mice were returned to their home cage with access to a running wheel and water *ad libitum* for at least 3 days before beginning of the experiment.

Virtual reality setup and behavioral paradigm

For all experiments we used a virtual reality setup as previously described (Leinweber et al., 2017). Mice were head-fixed and free to run on a spherical, air-supported styrofoam ball. Rotation of the ball was coupled to movement in a virtual reality environment. A virtual corridor was projected onto a toroidal screen positioned in front of the mice covering approximately 240 degrees horizontally and 100 degrees vertically of the field of view using a projector (Samsung SP-F10M). To prevent light leak from the projector onto the two-photon imaging plane, the projector was synchronized to the resonant scanner of the microscope. Mice were trained to control heading in the virtual tunnel and navigate toward a target. Upon reaching the target, a reward was delivered through a blunt syringe spout positioned near the snout of the mouse ($\sim$7 μL / reward, 1:10 diluted milk). To incentivize mice to engage in the training paradigm, they were water-restricted with access to 1 mL water daily 3 days before start of either imaging or optogenetic experiments. Care was taken to prevent a drop in body weight to below 80% of starting weight and additional water was supplemented when necessary. The amount of rewards the mice could collect during training was not restricted. A new trial was initiated after a 5 s time out during which a gray screen was presented. The tunnel was kept short initially (length to width ratio of 5:1) but was progressively lengthened to increase difficulty of the task such that mice collected approximately 2 rewards per minute. By the end of training, the tunnel length typically corresponded to approximately 4 m of physical distance (length to width ration of 30:1). Mice were trained and imaged daily in training sessions that lasted approximately 45 min. From training session three onward, visual offset perturbations were introduced with a probability of 0.8 per traversal at a random location in the virtual tunnel (restricted to the middle portion of the tunnel between 20% and 80% of total length). Visual offset perturbations consisted of a sudden 30° offset in the heading randomly either to the left or to the right.

Optogenetic inhibition experiments

Mice were trained to navigate the virtual environment as described above. Light from a 473 nm laser (Shanghai Laser & Optics Century, BL473H-200) was sinusoidally modulated at 40 Hz using a Pockels Cell (Conoptics, Model 350-80). The laser was directed at either two locations per hemisphere (in mm: 1.5 lateral, 0.5 and 1.5 anterior of bregma) at 5 mW time averaged power per location (10 mW per hemisphere), or one location (in mm: 1.5 lateral, 0.5 anterior of bregma) at 1 mW or 2 mW time averaged power per location/hemisphere. Full-width half maximum of the laser beam was 0.8 mm (pale blue dashed circle in Figure S1A) and power dropped to 1/e at a radius of 0.5 mm. Photostimulation was performed through a cranial window. We used a galvo-galvo scan head to either cycle between the target locations or between two blank locations on the head-bar during times of no stimulation. For stimulation, the laser cycled between each of the two (four) target locations for the duration of the stimulus with a dwell time of 40 ms (20 ms) per location. To minimize stimulation related changes in audible noise generated by the moving galvanometers and luminance changes associated with scanning of the laser beam, the laser was continuously cycled between the two blank locations on the head bar during times of no stimulation. For the chronic inhibition experiments during training (Figures 1, 2, S1, and S2), we stopped inhibition of motor cortex in cases where the trial lasted more than 15 s by cycling the laser between the blank positions.

Inhibition was then resumed at the start of the next trial. This was done to increase the motivation of the mice to run on the spherical treadmill. For the experiments on the effect of motor cortex inhibition on the response to visual offset perturbations in trained mice (Figures 2 and S2), the laser was switched from blank to target position at different times relative to the onset of the visual offset perturbation (−1 s, −0.5 s, 0 s, 0.5 s, 1 s). Different laser onset times were randomized and data were collected over four training sessions on four consecutive days.

Two-photon calcium imaging

All two-photon imaging experiments were performed using a modified Thorlabs B-Scope as described previously (Leinweber et al., 2017). Light source was a femtosecond laser (MaiTai eHP DeepSee, Spectra Physics) tuned to 990 nm. The scan head was based on an 8 kHz resonant scanner (Cambridge Technology). For imaging we used a 16x, 0.8 NA objective (Nikon). Emission light was band pass filtered (525/50, Semrock BrightLine) and detected using GaAsP photomultiplier tubes (H7422, Hamamatsu). Photomultiplier tube signals were amplified (DHPCA-100, Femto), digitized (NI5772, National Instruments) at 800 MHz and band-pass filtered at 80 MHz using a digital Fourier-transform filter implemented in custom written software on an FPGA (NI5772, National Instruments). Images were acquired at 40 Hz frame rate at a resolution of 750 × 400 pixels.

All the imaging in layer 2/3 and layer 5 IT neurons were done in cell bodies. In a subset of mice (3 of 11 mice), we recorded activity of layer 5 PT neurons from main dendritic trunks below the apical arborization, because the image quality did now allow for somata imaging (Figures S3A–S3C). We found no evidence for a difference in the effects we described between somatic or dendritic recordings of these layer 5 PT neurons (Figures S3D–S3F), and therefore pooled dendritic and somatic recordings for all subsequent analyses.

Histology

For histological processing at the end of the experiment, mice were deeply anesthetized with a ketamine-xylazine mixture, transcardially perfused with 4% PFA/PBS and brains were extracted and post-fixed for 24 hr. After cryopreservation in 30% sucrose/PBS, brains were frozen in embedding medium (Tissue-Tek) and stored at −80°C. Sections were then cut with a thickness of 80 μm using a cryostat, collected free-floating in PBS, and subsequently immuno-stained for GFP (ThermoFisher, RRID:AB_2534023) and the neuron-specific protein NeuN (Millipore, RRID:AB_2298772). Fluorophore-coupled secondary antibodies were obtained from Jackson or ThermoFisher. Stained sections were then mounted in a glycerol-based medium and imaged using a Zeiss LSM700 or a Visitron Spinning Disc confocal microscope.

QUANTIFICATION AND STATISTICAL ANALYSIS

Data analysis

All data analysis was performed using custom-written and publicly available (https://sourceforge.net/projects/iris-scanning) software written in MATLAB (MathWorks). Statistical tests were used as stated in the figure legends.

Behavioral data analyses

Onsets of spontaneous turns were determined by thresholding (0.12 deg/s) the absolute value of rotational velocity of the spherical treadmill. To isolate well-defined turns, we discarded turn onsets that were preceded by another turn in the same direction within 5 s. This excluded 45% of the turns identified with the threshold crossing criterion. This procedure was aimed at eliminating threshold crossings that occurred in rapid succession either as a result of noise in the recording or as small rotational velocity changes due to individual steps. Our results did not change qualitatively when varying this exclusion window size over a wide range (2 s - 10 s). Thus, for spontaneous turns neural and behavioral data were aligned to the threshold crossing of the rotational velocity as described above. For induced turns (Figures 2, 6, 7, 8, S2, S3, and S8), neural and behavioral data were aligned to the time of the visual offset perturbation. To measure the fraction of time spent running (Figures 1 and S1), we used a threshold of 0.6 cm/s on the forward velocity of locomotion of the mouse on the spherical treadmill.

Performance (Figures 1 and S1) was quantified as the fraction of time spent running toward the target (±36 degrees from the direction of the target) normalized by the total time spent running. Plateau performance was defined as the first day at which a mouse's performance reached 90% of its maximum performance. The learning rate (Figure S1) was calculated as the slope of a line fit to the performance data. Rotational acceleration during a spontaneous (induced) turn (Figure 2) was quantified as the difference in mean speed in a post window 0 s to 1 s (0.5 s – 1.5 s) and the mean speed in a baseline window - 2 s to - 1.5 s (- 0.5 s to 0 s) normalized by the time between the two windows. Note that we used the same baseline and response windows for both behavioral and neuronal (see below) quantifications. Spontaneous turns during optogenetic inhibition (Figure 2) were analyzed in expert mice, on performance testing days. To compare spontaneous and induced turning behavior with optogenetic inhibition from the same expert mice (Figure 2), we excluded one mouse of which we did not have data for induced turns. For the visual offset perturbation responses, delayed response trials (Figures 2 and S2) were defined as trials in which turning velocity of the mice did not cross a threshold (10 deg/s) within 1 s after visual offset perturbation.

Onsets of running (Figure S4) were determined by thresholding the forward locomotion velocity of the mouse on the spherical treadmill. To include only well isolated running onsets we used a threshold of 1.2 cm/s, and discarded running onsets that were preceded by running onset in a window of 2.5 s or were within 5 s of a reward delivery.

Calcium imaging data analyses

Raw two-photon images were full-frame registered to correct for brain motion. Neurons were manually selected based on mean and maximum fluorescence images. Note that the use of maximum fluorescence images biased our selection of neurons to active neurons. Other than excluding neurons that were not clearly identifiable in any of the imaging time points, we excluded no neurons from further analysis. Raw fluorescence traces (F) were computed and smoothed as previously described (Leinweber et al., 2017). $(F-F_0)/F_0$ (abbreviated as $\Delta F/F$) values were calculated using the median fluorescence (over the entire recording session) for normalization (F_0).

To compute the average event-triggered change in fluorescence $\Delta F/F$ (Figures 3, 4, S6–S8), we baseline subtracted the responses of each neuron using the baseline windows: for spontaneous turns −2 s to −1.5 s; for visual offset perturbation-induced turns, running onsets and air puffs −0.5 s to −0 s. To compute average responses (Figures 3, 4, 5, 6, 7, 8, and S3–S8) we used differences of mean $\Delta F/F$ in a response window and mean $\Delta F/F$ the baseline window. Response windows were: for spontaneous turn and air puff responses: 0 s to 1 s; for visual offset perturbation-induced turn and running onset responses: 0.5 s to 1.5 s.

We defined neurons as contraversive (ipsiversive) turn neurons (Figures 3, 5, 6, 7, 8, S3, S4, S6, and S8) if their response during contraversive (ipsiversive) turns was stronger than their response during ipsiversive (contraversive) turns. Note, in this way all neurons are either classified as contraversive or ipsiversive and no neurons excluded. To obtain a population response, we then calculated the average of the activity of contraversive turn neurons during contraversive turns and the average of ipsiversive turn neurons during ipsiversive turns, and then averaged these two responses (Figures 3, 5, 6, S3, S4, and S8). Note that the average learning related population response reported in Figure 4 does not take into account the neuron's preference for turning direction.

Linear trend analysis (Figures 2, 3, 6, S3, S4, and S8) was performed using the MATLAB regress function. To quantify the significance of the linear trend we report the R^2 statistic and p value of the F statistic.

To increase the number of turns in the lowest acceleration bin in Figures 3F, 3J, S3, S4, and S8, we did not apply the 5 s inter turn interval exclusion criterion for this bin.

Learning related change of correlation (Figures 4C and 4F) was calculated for each neuron as the absolute value of the Pearson's correlation coefficient of the rotational velocity of the treadmill and the fluorescence trace. To reduce the potential impact of movement artifacts in the fluorescence traces, which would lead us to overestimate the strength of correlation, we set all $\Delta F/F$ values below 1 to 0 before calculating the correlation coefficient.

Latency of activation during induced turns was estimated by first selecting neurons that had a significant response to visual offset perturbations in a window 0.5 s to 1.5 s after visual offset (response versus baseline window −0.5 s to 0 s preceding the visual offset, $p < 10^{-3}$, Student's t test). For these neurons we then detected in an early response window (0 s - 0.3 s after visual offset) the first time point at which the fluorescence trace crossed a threshold of 2 standard deviations of the fluorescence distribution in a window −0.5 s to 0 s preceding visual offset.

The duration of the concurrent activation during contra- and ipsiversive turns in response to visual offset perturbations (Figure 7E) was estimated for all neurons by determining the first significant difference between ipsi- and contraversive responses in a window 0 s to 1.25 s after visual offset. Threshold for significant responses was twice the standard deviation of the difference in a window −0.5 s to 0 s preceding visual offset.

For the analysis of stability of responses over the course of training (Figure S5) we calculated a matrix of Pearson's correlation coefficients of neuronal population response vectors during contra- and ipsiversive turns separately. Data of each day was split into first and second half, and the correlation matrix obtained by correlating the population vector obtained from the first half of the data on day A with the population vector obtained from the second half of the data on day B. The time constant of the stability of the neuronal response was approximated by the decay constant of an exponential fit through the mean values of the off-diagonals of the correlation matrix.

For the analysis of differences of activation during spontaneous turns as a function of direction of the turn (Figures 5 and S6), turns were classified as directed toward the target or as directed away from the target and binned by the heading relative to the target preceding the onset of the turn (average heading in a window −0.625 s to −0.125 s preceding the turn onset). To acceleration-match turns toward and away from the target for each heading bin separately, we sorted all turns by the average acceleration in a window 0 s to 1 s after turn onset. We then successively excluded the highest acceleration turns in the heading bin with the higher average acceleration and the lowest acceleration turns in the heading bin with the lower average acceleration until the heading bin that initially had the higher average acceleration had a lower average acceleration than the heading bin that initially had the lower average acceleration. This was done in steps of 1% of the number of turns.

The time course of population vector correlation (Figures 7, S7, and S8) was obtained by calculating the average Pearson's correlation of the population vector of activity during ipsi- and contraversive turns for all mice. The population vector of activity was calculated as a function of time, averaging the activity in a window of 0.4 s in steps of 0.2 s. To account for differences in the number of turns per mouse we randomly sub-selected an equal number of turns (corresponding to number of turns from the mouse with the least turns) from all mice. To obtain estimates of the baseline level of correlation, we computed the population vector of activity correlation at random times during running. To visualize the dynamics of the population vector of activity around spontaneous and induced turn onsets (Figures 8 and S8), we projected the population vector of activity for each turn event, calculated in time bins of 0.1 s, onto the two-dimensional space spanned by the population vector during a spontaneous right turn and the population vector during a spontaneous left turn (calculated as the difference between 0 s and 1 s after turn onset). This was done for spontaneous

contra- and ipsiversive, and induced contra- and ipsiversive turns separately. For this analysis, data from mice with less than 15% contraversive or ipsiversive neurons were excluded (0 of 8 layer 2/3 mice and 2 of the 11 layer 5 PT mice), as in these mice the estimate of spontaneous turn basis vectors was too unstable. The onsets of the behavioral response for the induced turns (Figures 8 and S8, black crosses) were estimated as the time bin with first significant ($p < 0.05$, Student's t test) deviation of the distribution of rotational velocity after the visual offset perturbation (in a window of 25 ms, measured in steps of 25 ms) from the distribution immediately preceding the visual offset perturbation (in a window of 25 ms).

DATA AND SOFTWARE AVAILABILITY

Requests for data and software should be directed to and will be fulfilled by the Lead Contact, Georg Keller (georg.keller@fmi.ch). Software for controlling the two-photon microscope and preprocessing of the calcium imaging data is available on https://sourceforge.net/projects/iris-scanning/.

Neuron, Volume *99*

Supplemental Information

Mouse Motor Cortex Coordinates the Behavioral Response to Unpredicted Sensory Feedback

Matthias Heindorf, Silvia Arber, and Georg B. Keller

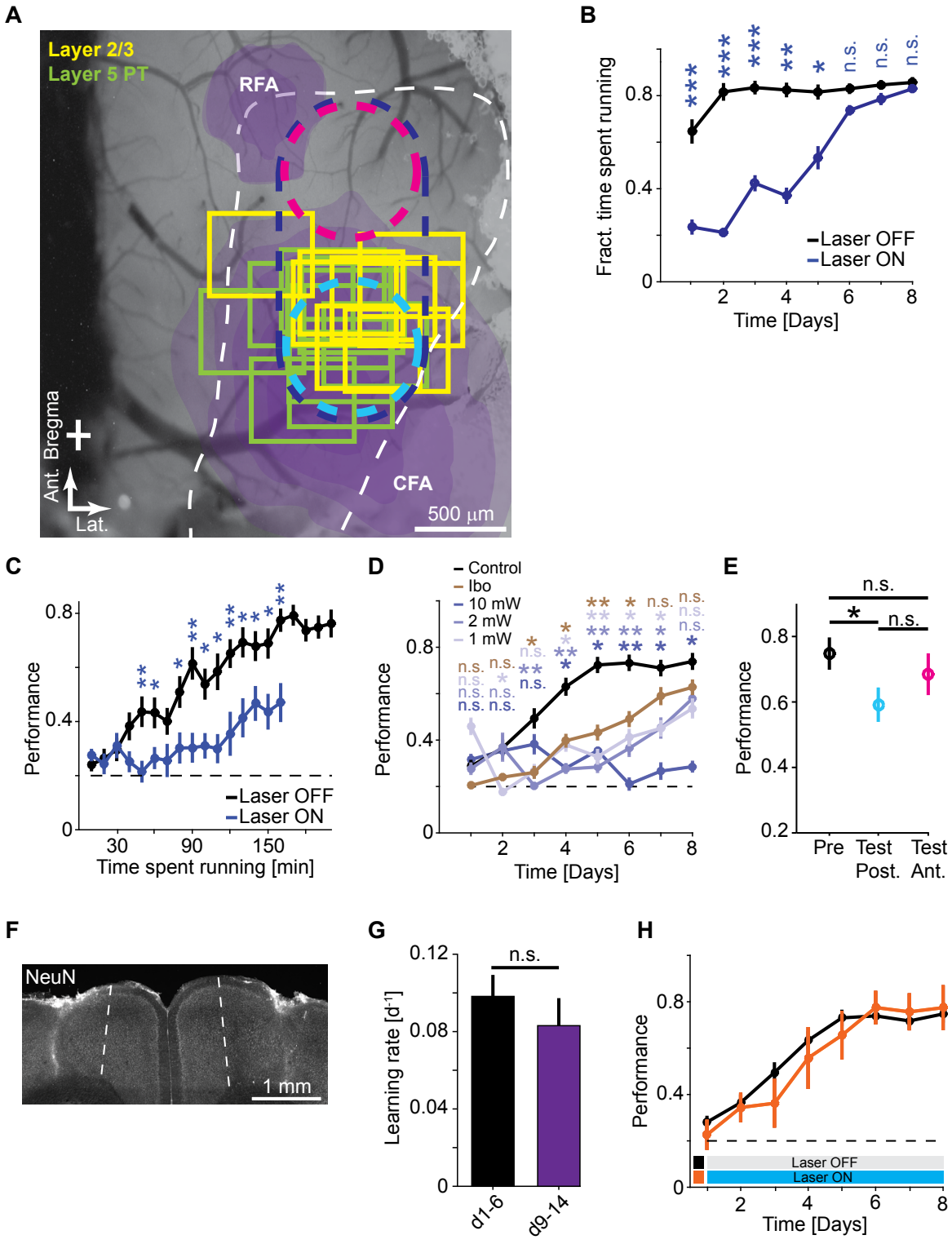
A
Layer 2/3
Layer 5 PT
RFA
CFA
Ant.
Bregma
Lat.
500 µm
B
Fract. time spent running
Time [Days]
Laser OFF
Laser ON
C
Performance
Time spent running [min]
Laser OFF
Laser ON
D
Control
Ibo
10 mW
2 mW
1 mW
Performance
Time [Days]
E
Performance
Pre
Test Post.
Test Ant.
F
NeuN
1 mm
G
Learning rate [d-1]
d1-6
d9-14
H
Performance
Time [Days]
Laser OFF
Laser ON

Figure S1. Inhibition of CFA reduces task performance – additional information and controls. Related to Figure 1.

(**A**) Approximate location of the imaging fields of view (550 µm x 450 µm) in layer 2/3 (yellow, n = 8 mice) and layer 5 PT (green, n = 11 mice) experiments superimposed on an example wide-field fluorescence image of motor cortex. Dashed dark blue oval marks full-width half maximum of the laser beam at the surface of cortex (10 mW average power per hemisphere, see STAR Methods) at the endpoints of the scan during optogenetics experiments. Purple shading marks the caudal forelimb area (CFA) and the rostral forelimb area (RFA) in motor cortex (dashed white line); adapted from (Tennant et al., 2011). Dashed blue and pink circles mark optogenetic stimulation locations for inhibition experiments targeted at the CFA or a more anterior region in motor cortex, at 1 mW and 2 mW average power per hemisphere. Ant.: anterior; Lat.: lateral; white cross marks bregma.

(**B**) Fraction of time spent running without (black, n = 22 mice) and with (blue, n = 12 mice) bilateral inhibition of motor cortex as a function of training days. Fraction of time spent running was higher without inhibition of motor cortex. Error bars indicate SEM over mice. n.s.: not significant, *: $p < 0.05$, **: $p < 0.01$, ***: $p < 10^{-3}$; Wilcoxon rank sum test between groups.

(**C**) Performance as a function of time spent running for the first 8 days of training. Same coloring as in **B**. Error bars indicate SEM over mice. Dashed black line marks chance performance. *: $p < 0.05$, **: $p < 0.01$; Wilcoxon rank sum test between groups.

(**D**) Quantification of the average performance as a function of training days, laser power and stimulus location (as outlined in **A**, see STAR Methods) in mice with (dark blue, rostral and caudal location, 10 mW, n = 3 mice; intermediate blue, caudal location, 2 mW, n = 5 mice; pale blue, caudal location, 1 mW, n = 4 mice) or without (black, n = 22 mice) motor cortex inhibition or chronic ibotenic acid micro-lesions (Ibo, brown, n = 5 mice). Note that using lower laser power centered on the CFA still significantly impaired learning. Dashed black line marks chance performance. n.s.: not significant, *: $p < 0.05$, **: $p < 0.01$; Wilcoxon rank sum test vs control group.

(**E**) The effect of decrease in performance in expert mice was larger when optogenetically inhibiting the posterior location (CFA, cyan) than when inhibiting the anterior location (pink). Error bars indicate SEM over mice (n = 9 mice). *: $p < 0.05$, n.s.: not significant; Wilcoxon rank sum test.

(**F**) Confocal image of a bilateral chronic ibotenic acid micro-lesion of the CFA in a *C57/Bl6* mouse. Coronal slice is 0.5 mm anterior or bregma. Dashed lines mark medial CFA boundaries.

(**G**) Learning rate in **Figure 1C** days 1 to 6 for mice without inhibition of motor cortex (black, n = 22 mice) and days 9 to 14 for mice with bilateral inhibition of motor cortex (purple, n = 3 mice). Error bars indicate SEM over mice. n.s.: not significant; $p = 0.42$; Wilcoxon rank sum test.

(**H**) Performance of *C57BL/6* mice that received blue laser stimulation in motor cortex during training, but did not express channelrhodopsin-2 in vGAT+ interneurons (n = 4 mice, orange line), compared to mice that were trained without blue laser (n = 22 mice, black line). Error bars indicate SEM over mice. Dashed black line marks chance performance.

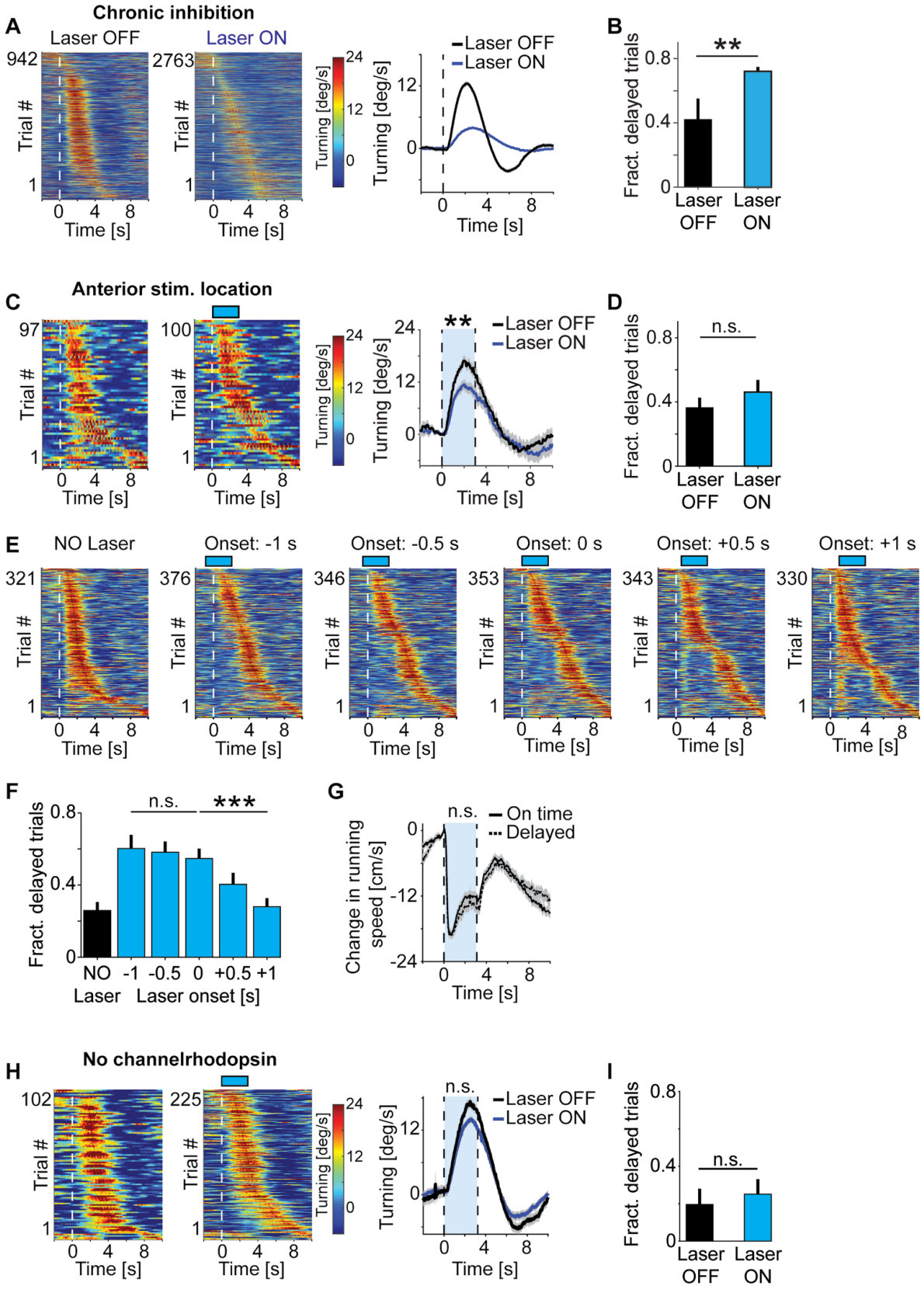
A
Chronic inhibition
Laser OFF
Laser ON
942
2763
Trial #
Time [s]
Turning [deg/s]
Laser OFF
Laser ON
B
Fract. delayed trials
**
Laser OFF
Laser ON
C
Anterior stim. location
97
100
**
D
n.s.
E
NO Laser
Onset: -1 s
Onset: -0.5 s
Onset: 0 s
Onset: +0.5 s
Onset: +1 s
321
376
346
353
343
330
F
n.s.
***
NO Laser
-1
-0.5
0
+0.5
+1
Laser onset [s]
G
n.s.
On time
Delayed
Change in running speed [cm/s]
H
No channelrhodopsin
102
225
I
n.s.

Figure S2. Channelrhodopsin-2 mediates impairment during photoinhibition. Related to Figure 2.

(**A**) Responses to visual offset perturbations were greatly reduced during chronic bilateral inhibition of motor cortex. Left panel: Turning velocity response to 942 visual offset perturbations in 3 mice during training days 3 to 8 without chronic inhibition of motor cortex, sorted by time to peak velocity. Middle panel: Turning velocity response to 2763 visual offset perturbations in 12 mice (data from all three inhibition power levels 1 mW, 2 mW, and 10 mW combined) during training days 3 to 8 with chronic bilateral inhibition of motor cortex, sorted by time to peak velocity. Color indicates turning speed. Right panel: Average speed profile for the data shown in left and middle panels. Shading indicates SEM over turns.

(**B**) Fraction of delayed turns (see STAR Methods) without (left, black) or with (right, cyan) chronic photoinhibition. Same data as in **A**. Error bars indicate SEM over mice. **: $p < 0.01$; Wilcoxon rank sum test.

(**C**) Speed profile of 97 visual offset perturbation-induced corrective turns in expert mice that had reached plateau performance without (left panel, n = 9 mice) and with (middle panel, 100 trials, n = 9 mice) bilateral inhibition of anterior motor cortex (pink circle in **Figure S1A**) concurrent with visual offset perturbation for 3 s (blue bar). Turns are sorted by latency to peak velocity. Right panel: Average speed profile for the data shown in left and middle panels. Shading indicates SEM over turns. **: $p < 0.01$; Wilcoxon rank sum test.

(**D**) Fraction of delayed turns (see STAR Methods) without (left, black) photoinhibition or with (right, cyan) photoinhibition concurrent with visual offset perturbation. Same data as in **C**. Error bars indicate SEM over mice (n = 9 mice). n.s.: not significant; Wilcoxon rank sum test.

(**E**) Turning responses to visual offset perturbations during different inhibition onset times relative to visual offset perturbation, sorted by time to peak velocity. Data were collected in expert mice that had received at least 8 training sessions. Stimulation onset and duration indicated by blue bar. Color indicates turning speed as in **A**.

(**F**) Fraction of delayed turns (see STAR Methods) as a function of the timing of laser inhibition onset relative to the visual offset perturbation (data from all three inhibition power levels 1 mW, 2 mW, and 10 mW combined). Error bars indicate SEM over mice (n = 14 mice). ***: $p < 10^{-3}$, n.s.: not significant; Wilcoxon rank sum test.

(**G**) Reduction of running speed induced by concurrent inhibition of motor cortex and visual offset perturbation for trials in which mice executed an induced turn on time (solid black line, n = 144) and for trials in which mice delayed the induced turn until the offset of the inhibition of motor cortex (dashed black line, n = 209). Trials are same as in **E**, 0 s onset. Blue bar marks duration of motor cortex inhibition (0 s to 3 s). Shading indicates SEM over trials. n.s.: not significant; Wilcoxon rank sum test.

(**H**) Speed profile of visual offset perturbation-induced corrective turns in mice that did not express channelrhodopsin-2 in vGAT+ interneurons without (left panel, 102 turns, n = 5 mice) and with (middle panel, 225 turns, n = 5 mice) blue laser stimulation of motor cortex concurrent with visual offset perturbation for 3 s (blue bar). Data are from expert mice with at least 8 training sessions. Trials are sorted by latency to peak turning velocity. Color indicates turning speed. Right panel: Average speed profile for the data shown in left and middle panels. Shading indicates SEM over turns. n.s.: not significant; Wilcoxon rank sum test.

(**I**) Fraction of delayed turns (see STAR Methods) in mice (n = 5 mice) that did not express channelrhodopsin-2 in vGAT+ interneurons without (black) or with blue laser stimulation of motor cortex concurrent with visual offset perturbation (blue). Error bars indicate SEM over mice. n.s.: not significant; Wilcoxon rank sum test.

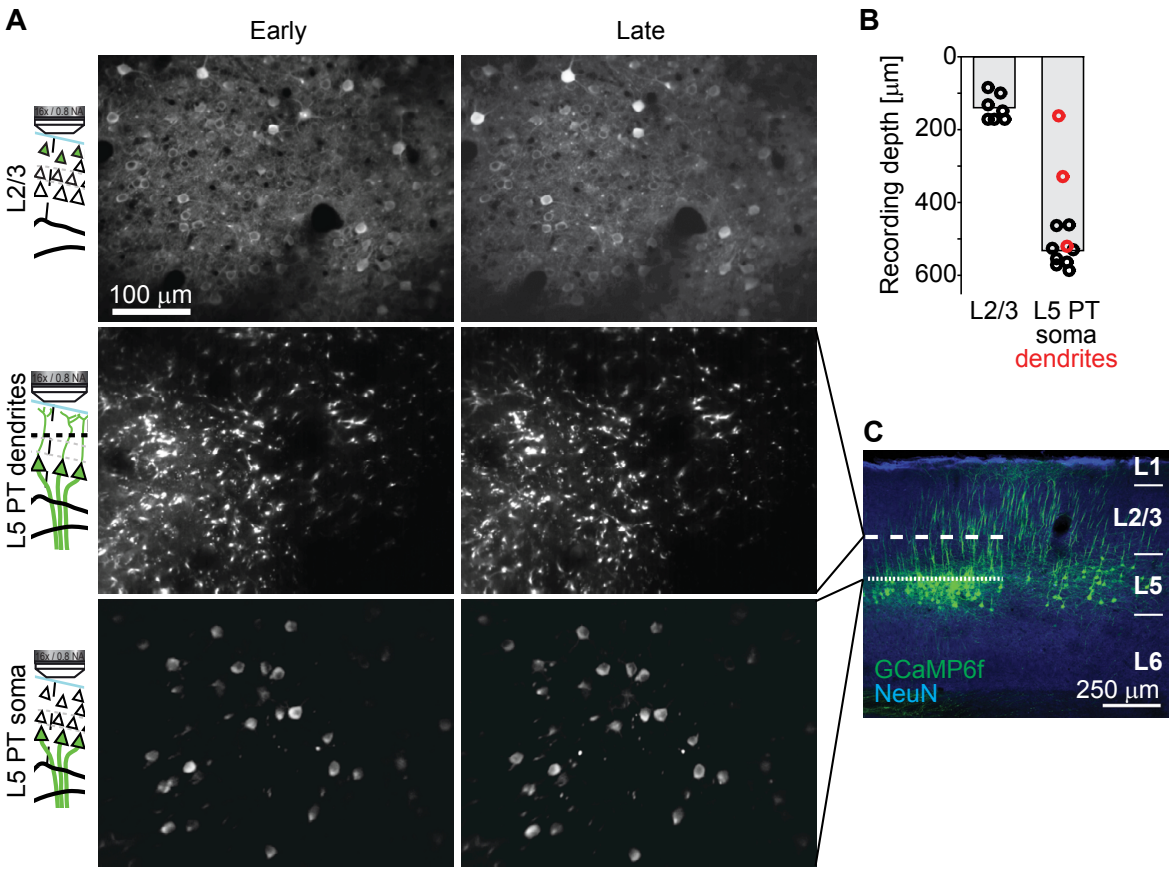
A
Early
Late
L2/3
L5 PT dendrites
L5 PT soma
100 µm
B
Recording depth [µm]
0
200
400
600
L2/3
L5 PT soma
dendrites
C
L1
L2/3
L5
L6
GCaMP6f
NeuN
250 µm

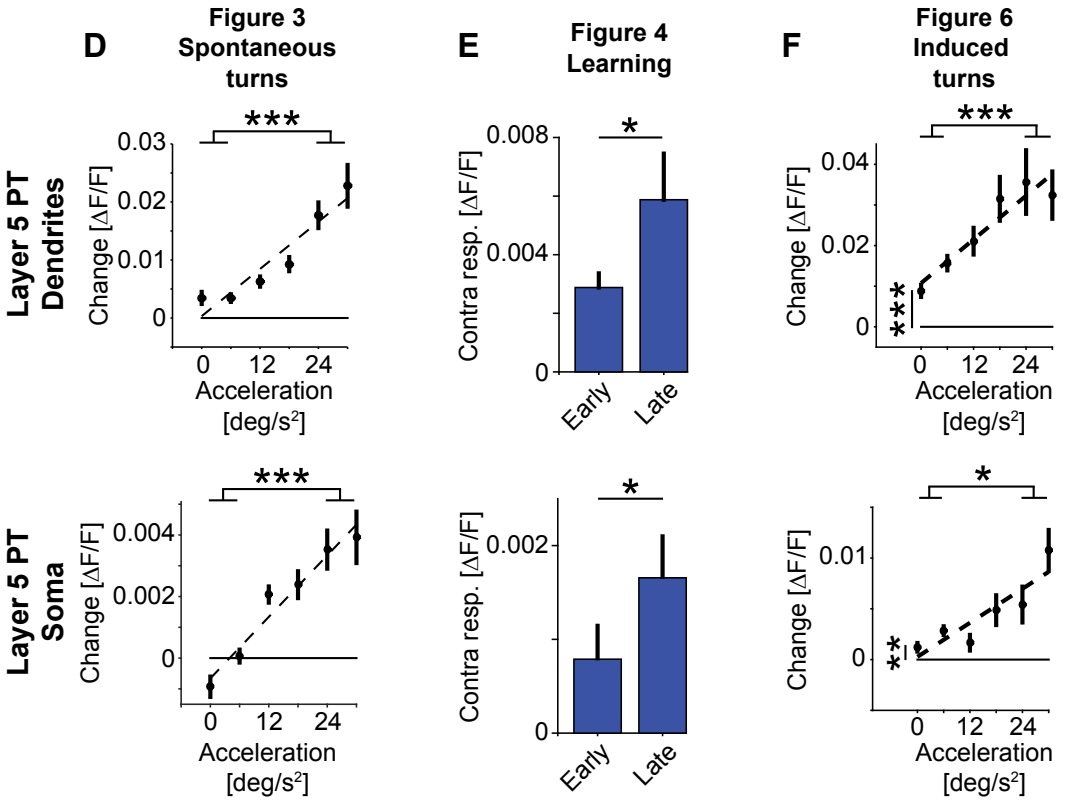
Figure 3
Spontaneous turns
Figure 4
Learning
Figure 6
Induced turns
D
E
F
Layer 5 PT Dendrites
Layer 5 PT Soma
Change [ΔF/F]
Contra resp. [ΔF/F]
Acceleration [deg/s²]
Early
Late
***
*
**

Figure S3. Data recorded from layer 5 PT dendrites and layer 5 PT soma are qualitatively comparable. Related to Figure 3.

(**A**) Sample two-photon maximum projections of the same layer 2/3 (top row), layer 5 PT soma (middle row) and layer 5 PT dendrite recordings early (left column) and late (right column) in the course of training.

(**B**) Depth of recording below the pial surface of cortex for the layer 2/3 recordings and the layer 5 PT recordings. Each dot corresponds to one imaging site. In red are the recording sites in which we imaged dendrites of layer 5 PT neurons because imaging quality at the somata was not sufficient for data analysis.

(**C**) Confocal image of layer 5 PT neurons in motor cortex of a *Sim1(KJ18)-Cre* mouse injected with AAV2/1-EF1α-DIO-GCaMP6f. White dashed line and white dotted line indicate approximate locations of layer 5 PT dendrites and layer 5 PT soma recordings, respectively, as shown in **A**.

(**D**) Comparison of the scaling of the response with acceleration of spontaneous turns (as in **Figure 3J**) in dendrites and somata separately. Error bars indicate SEM over the number of compartments. ***: $p < 10^{-3}$, n = 224 somata and 336 dendrites; paired Student's t test.

(**E**) Comparison of the increase of neuronal activity in response to contraversive turns (as in **Figure 4E**) in dendrites and somata separately. Error bars indicate SEM over the number of compartments. *: $p < 0.05$, n = 224 somata and 336 dendrites; paired Student's t test.

(**F**) Comparison of the scaling of the response with acceleration of induced turns (as in **Figure 6F**) in dendrites and somata separately. Error bars indicate SEM over the number of compartments. *: $p < 0.05$, ***: $p < 10^{-3}$, n = 224 somata and 336 dendrites; paired Student's t test.

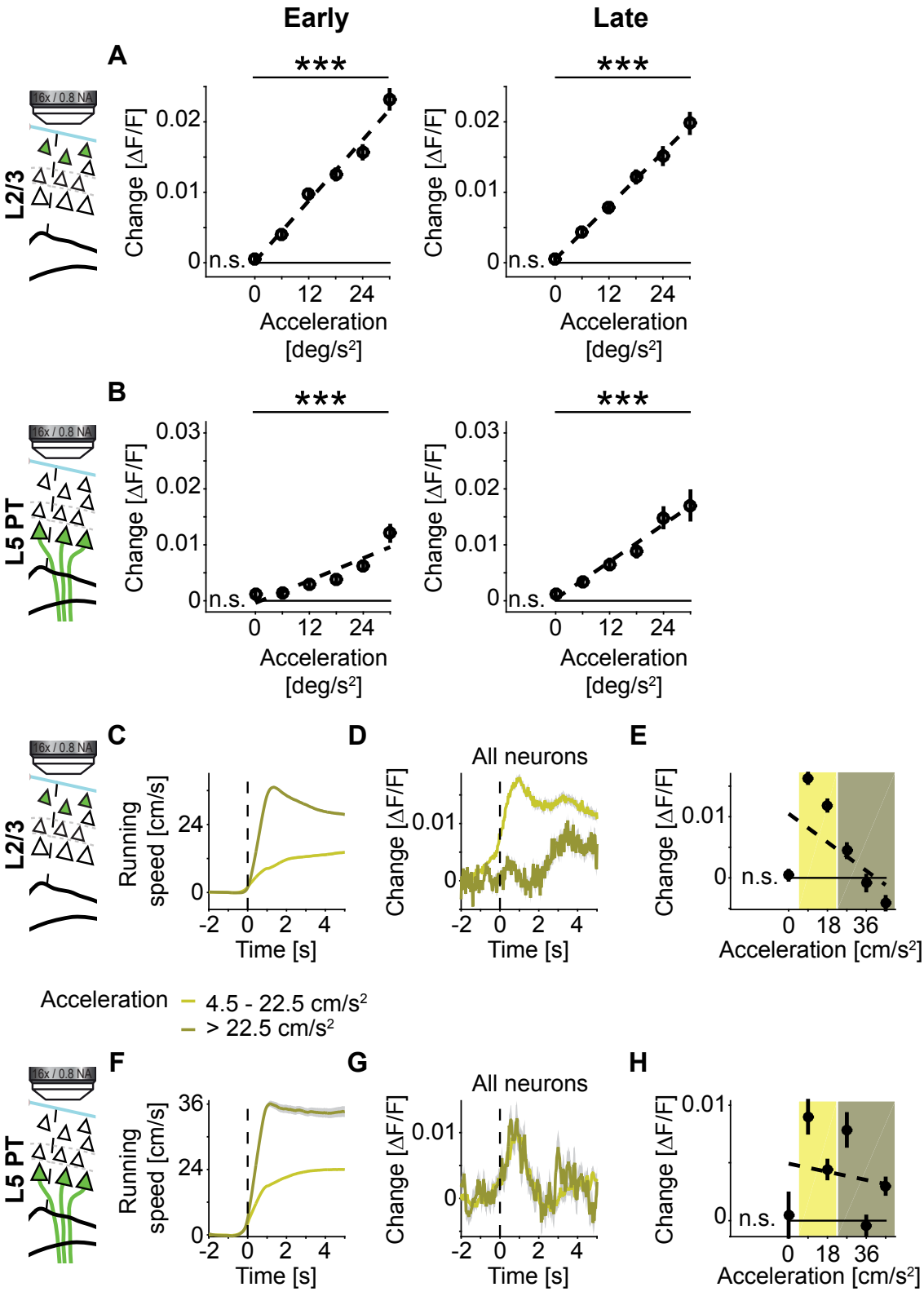
Early
Late
A
***
***
16x / 0.8 NA
L2/3
Change [ΔF/F]
0.02
0.01
0
n.s.
0
12
24
Acceleration
[deg/s²]
B
***
***
16x / 0.8 NA
L5 PT
Change [ΔF/F]
0.03
0.02
0.01
0
n.s.
0
12
24
Acceleration
[deg/s²]
C
D
E
16x / 0.8 NA
L2/3
Running
speed [cm/s]
24
0
-2
0
2
4
Time [s]
All neurons
Change [ΔF/F]
0.01
0
-2
0
2
4
Time [s]
Change [ΔF/F]
0.01
0
n.s.
0
18
36
Acceleration [cm/s²]
Acceleration
4.5 - 22.5 cm/s²
> 22.5 cm/s²
F
G
H
16x / 0.8 NA
L5 PT
Running
speed [cm/s]
36
24
0
-2
0
2
4
Time [s]
All neurons
Change [ΔF/F]
0.01
0
-2
0
2
4
Time [s]
Change [ΔF/F]
0.01
0
n.s.
0
18
36
Acceleration [cm/s²]

Figure S4. Activity scales linearly with spontaneous turn amplitude in both early and late phases of training, but not with acceleration during running initiation. Related to Figure 3.

(**A**) Activity of layer 2/3 neurons scales linearly with the acceleration of the turn both early (days 1 to 4, left) and late (days 5 to 8, right) in training. Error bars indicate SEM over neurons (n = 1154 neurons). ***: $p < 10^{-3}$, early: $R^2 = 0.07$, late: $R^2 = 0.04$, n = 1154 neurons; linear trend analysis (see STAR Methods). n.s.: not significant; Student's t test.

(**B**) Same as **A**, but for layer 5 PT neurons (n = 560 neurons). Early: $R^2 = 0.05$, late: $R^2 = 0.03$, n = 560 neurons; linear trend analysis (see STAR Methods).

(**C**) We split running onsets detected throughout training (days 1 to 8) into bins of high (dark yellow) and low (light yellow) acceleration. Shading indicates SEM over running onsets (number of high acceleration onsets: n = 901; low acceleration onsets: n = 1485).

(**D**) Average population activity of layer 2/3 neurons for the running onsets shown in **C** (n = 1154 neurons). Using the same binning as in **C**, the average neuronal activity was higher during running onsets of low acceleration. Colors as in **C**. Shading indicates SEM over neurons.

(**E**) Average population activity for layer 2/3 neurons (n = 1154 neurons) as a function of acceleration of the running onset. Error bars indicate SEM over neurons. Dashed black line is a linear fit to the data. n.s.: not significant, lowest bin is not different from zero; Student's t test.

(**F**) As in **C**, but for the layer 5 PT experiments (number of high acceleration onsets: n = 131; low acceleration onsets: n = 1914).

(**G**) As in **D**, but for layer 5 PT neurons (n = 560 neurons).

(**H**) As in **E**, but for layer 5 PT neurons.

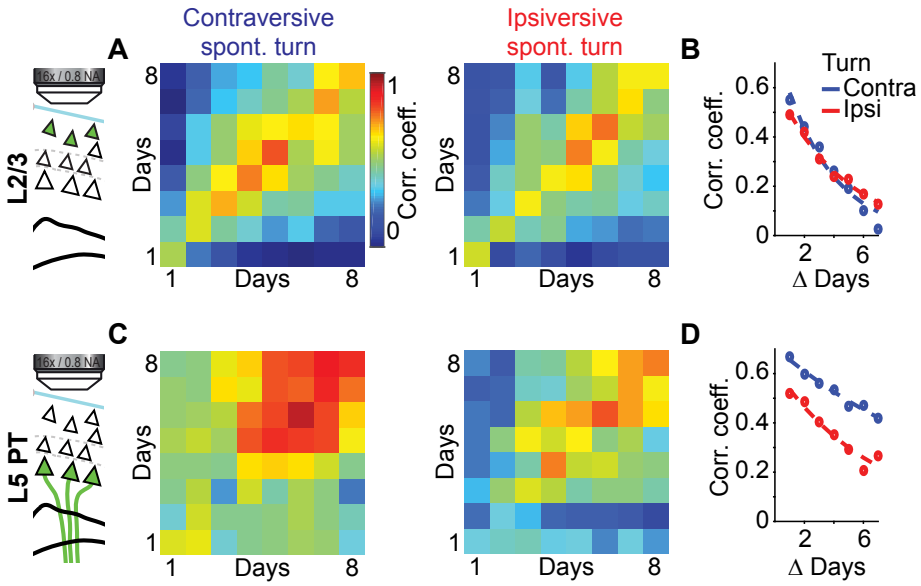

Figure S5. Activity during spontaneous turns is more stable in layer 5 PT over the course of training. Related to Figure 4.

(**A**) Stability of layer 2/3 population activity during contraversive (left) and ipsiversive turns (right). Data of each training day was split into first and second half and mean population vectors to contra- and ipsiversive turns computed from both halves. Shown is the average Pearson's correlation coefficient of the population vector (n = 1154 neurons) computed from the first half of the data (x-axis) with the population vector computed from the second half of the data (y-axis) as a function of days of training. Color indicates Pearson's correlation coefficient.

(**B**) Average Pearson's correlation coefficients of population vectors for contraversive (blue) and ipsiversive (red) turns as a function of the time difference in training days. Dashed lines are exponential fits to the data. Decay time constants are 3.3 and 4.6 days for contra- and ipsiversive turns, respectively.

(**C**) As in **A**, but for layer 5 PT neurons (n = 560 neurons).

(**D**) As in **B**, but for layer 5 PT neurons (n = 560 neurons). Decay time constants are 13.6 and 6.9 days for contra- and ipsiversive turns, respectively. Dashed lines are exponential fits to the data.

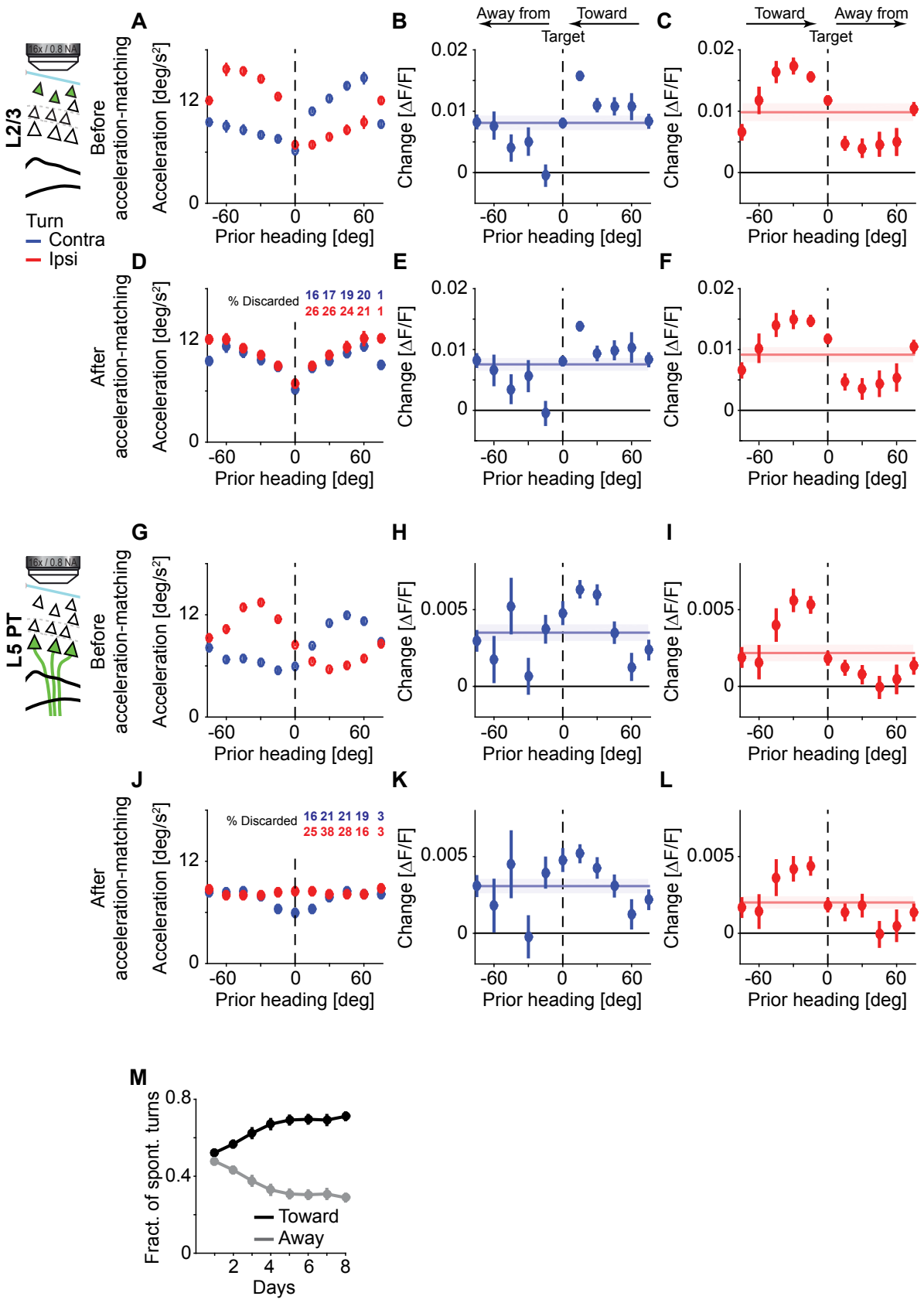
A
B
C
D
E
F
G
H
I
J
K
L
M
16x / 0.8 NA
L2/3
L5 PT
Before acceleration-matching
After acceleration-matching
Turn
Contra
Ipsi
Acceleration [deg/s²]
Change [ΔF/F]
Prior heading [deg]
Away from
Toward
Target
% Discarded
16 17 19 20 1
26 26 24 21 1
16 21 21 19 3
25 38 28 16 3
Fract. of spont. turns
Toward
Away
Days

Figure S6. Acceleration-matching of turns toward and away from target. Related to Figure 5.

(**A**) Average acceleration of the turn binned to heading prior to spontaneous turn onset for contraversive (blue) and ipsiversive (red) turns, before acceleration-matching. Data recorded throughout training (days 1 to 8) were used in this analysis. On average, turns toward the target are executed at higher acceleration than turns away from the target. A prior heading of 0 (dashed line) marks direction of target. Error bars indicate SEM over turns.

(**B**) Average activity of contraversive layer 2/3 neurons (n = 616 neurons) during contraversive spontaneous turns as a function of heading preceding the turn, before acceleration-matching. Data recorded throughout training (days 1 to 8) were pooled. Error bars indicate SEM over turns. Horizontal blue line and shading indicate the average response and SEM over turns. Solid black line marks 0 $\Delta F/F$.

(**C**) As in **B**, but for ipsiversive neurons (n = 538 neurons) and ipsiversive turns.

(**D**) As in **A**, with bins acceleration-matched pairwise around 0 degrees prior heading (see STAR Methods). Numbers at the top indicate the percentage of data that were discarded for each bin pair by the acceleration-matching procedure.

(**E**) As in **B**, but for acceleration-matched contraversive turns.

(**F**) As in **C**, but for acceleration-matched ipsiversive turns.

(**G**) As in **A**, but for layer 5 PT data set.

(**H**) As in **B**, but for contraversive layer 5 PT neurons (n = 229 neurons).

(**I**) As in **C**, but for ipsiversive layer 5 PT neurons (n = 331 neurons).

(**J**) As in **D**, but for layer 5 PT data set.

(**K**) As in **E**, but for contraversive layer 5 PT neurons.

(**L**) As in **F**, but for ipsiversive layer 5 PT neurons.

(**M**) Fraction of spontaneous turns that are taken toward (black) or away (gray) from target as a function of imaging days. Error bars indicate SEM over mice (n = 19 mice).

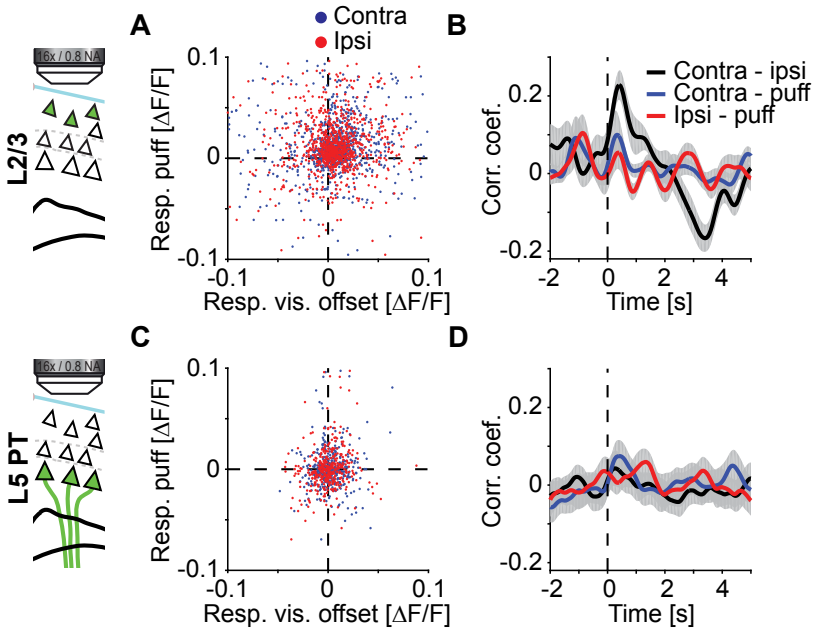

Figure S7. Visual perturbation offset responses do not correlate with air puff responses.

(**A**) Scatter plot of the average visual offset perturbation response recorded throughout training (days 3 to 8) versus the average air puff response for contra- (blue) and ipsiversive (red) layer 2/3 neurons. Each dot represents the response of an individual neuron (n = 973 neurons).

(**B**) Pearson's correlation coefficient of the population vector of layer 2/3 neurons (n = 973 neurons) during air puff stimulus and either contra- (blue) or ipsiversive (red), or contra- and ipsiversive (black) visual offset perturbation-induced turns, respectively, as a function of time around event onset. Gray shading marks an estimate of standard deviation (see STAR Methods).

(**C**) As in **A**, but for layer 5 PT neurons (n = 394 neurons).

(**D**) As in **B**, but for layer 5 PT neurons (n = 394 neurons).

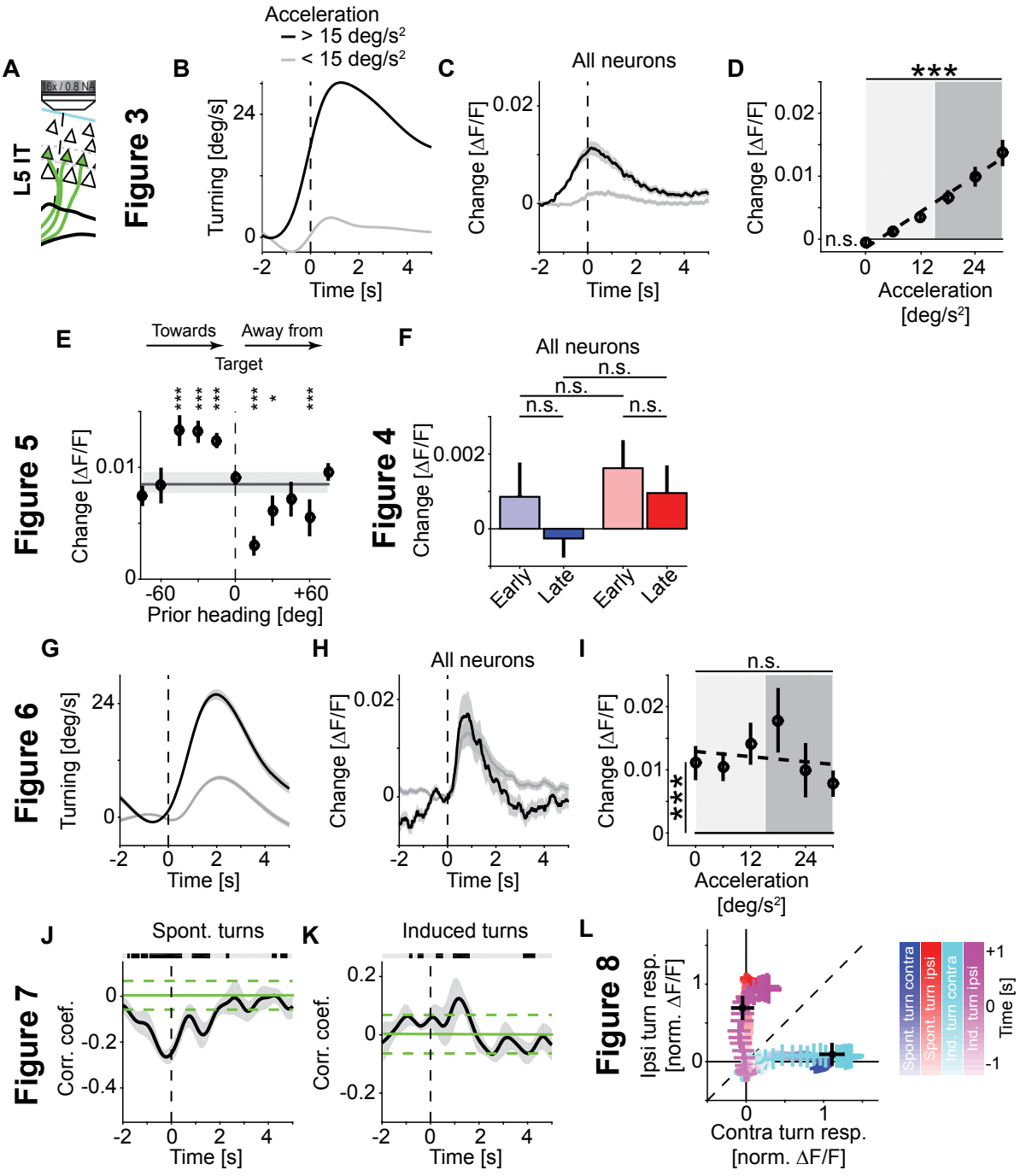
A
16x / 0.8 NA
L5 IT
Figure 3
B
Acceleration
> 15 deg/s²
< 15 deg/s²
Turning [deg/s]
24
0
-2 0 2 4
Time [s]
C
All neurons
Change [ΔF/F]
0.02
0
-2 0 2 4
Time [s]
D
***
Change [ΔF/F]
0.02
0.01
0
n.s.
0 12 24
Acceleration [deg/s²]
E
Towards
Away from
Target
Change [ΔF/F]
0.01
0
-60 0 +60
Prior heading [deg]
Figure 5
F
All neurons
n.s.
n.s.
n.s.
n.s.
Change [ΔF/F]
0.002
0
Early
Late
Early
Late
Figure 4
G
Turning [deg/s]
24
0
-2 0 2 4
Time [s]
H
All neurons
Change [ΔF/F]
0.02
0
-2 0 2 4
Time [s]
I
n.s.
Change [ΔF/F]
0.02
0.01
0
***
0 12 24
Acceleration [deg/s²]
Figure 6
J
Spont. turns
Corr. coef.
0
-0.2
-0.4
-2 0 2 4
Time [s]
K
Induced turns
Corr. coef.
0.2
0
-0.2
-2 0 2 4
Time [s]
Figure 7
L
Ipsi turn resp. [norm. ΔF/F]
1
0
0 1
Contra turn resp. [norm. ΔF/F]
Spont. turn contra
Spont. turn ipsi
Ind. turn contra
Ind. turn ipsi
+1
0
-1
Time [s]
Figure 8

Figure S8. Layer 5 IT neurons exhibit properties intermediate to those observed in layer 2/3 and layer 5 PT neurons.

(**A**) Schematics of the imaging experiments in layer 5 intratelencephalic (IT) projection neurons. To record the activity of layer 5 IT neurons we injected conditional AAV2/1-DIO-EF1α-GCaMP6f into *Tlx3(PL56)-Cre* mice (n = 9 mice).

(**B**) We split all spontaneous turns executed throughout training (days 1 to 8) into bins of high (black line) and low (gray line) acceleration. Shading indicates SEM over turns (number of turns for high acceleration bin: n = 7969; low acceleration bin: n = 8202).

(**C**) Larger turns were associated with higher neuronal activity. Average population activity of layer 5 IT neurons for the turns shown in **B** (n = 308 neurons). Colors as in **B**. Shading indicates SEM over neurons.

(**D**) Average population activity for layer 5 IT neurons as a function of acceleration of the spontaneous turn. Error bars indicate SEM over neurons (n = 308 neurons). Dashed black line is a linear fit to the data. Shading marks bins used for the turning and activity traces in **B** and **C**. ***: $p < 10^{-3}$, $R^2 = 0.06$, n = 308 neurons; linear trend analysis (see STAR Methods). n.s.: not significant, lowest bin is not different from zero; Student's t test.

(**E**) Average activity during spontaneous turns in layer 5 IT neurons as a function of the heading in a window -0.625 s to -0.125 s preceding the turn. Turns executed throughout training (days 1 to 8) were acceleration-matched (see STAR Methods) and binned such that a negative prior heading indicates a turn toward the target and a positive prior heading a turn away from the target. Error bars indicate SEM over turns. Horizontal gray line and shading indicate the average response and SEM over turns. *: $p < 0.05$, ***: $p < 10^{-3}$; Student's t test against the center bin. Bins that are not significant are not marked.

(**F**) Average layer 5 IT responses during contraversive (blue) and ipsiversive (red) turns early (days 1 to 4) and late (days 5 to 8) in training. Responses during neither contraversive nor ipsiversive turns changed with training. Error bars indicate SEM over neurons (n = 308 neurons). n.s.: not significant; paired Student's t test.

(**G**) We split visual offset perturbation-induced turns recorded throughout training (days 3 to 8) into bins of high (black line) and low (gray line) acceleration. Shading indicates SEM over turns (number of turns for high acceleration bin: n = 421; low acceleration bin: n = 1038).

(**H**) Average response in layer 5 IT neurons for the high (black line) and low (gray line) acceleration turns as defined in **G**. Both low and high acceleration turns result in almost identical activation of layer 5 IT neurons (n = 308).

(**I**) Average population response of layer 5 IT neurons as a function of acceleration of the induced turn. Error bars indicate SEM over neurons (n = 308 neurons). Dashed black line is a linear fit to the data. Shading marks bins used for the turning and activity traces in **G** and **H**. ***: $p < 10^{-3}$, Student's t test of first bin versus no response; n.s.: not significant, paired Student's ttest of first vs last bin. We found no evidence of a linear trend ($p = 0.8$, $R^2 = 0.003$, n = 308 neurons; linear trend analysis, see STAR Methods).

(**J**) Pearson's correlation coefficient of the population vector during contraversive and ipsiversive turns as a function of time around turn onset (black line, gray shading marks standard deviation over turns). Horizontal green lines mark mean (solid) and standard deviation (dashed) of random correlation. Horizontal black line marks time bins in which correlation is significantly different from chance (gray indicates bins that are not significant).

(**K**) Same as **J**, but for visual offset perturbation-induced turns.

(**L**) We projected the population vector activity of layer 5 IT neurons onto the plane spanned by the population vector 1 s after turn onset during spontaneous contraversive and spontaneous ipsiversive turns. Origin of the coordinate system is the mean population vector preceding turns. We first projected the population vector during spontaneous contraversive (blue) and spontaneous ipsiversive (red) turns executed throughout training (days 1 to 8) onto this coordinate system. By design projections start at the origin and peak at 1 on their axis. Shading of the maker indicates time relative to turn onset. We then projected the population activity vector during induced contraversive (cyan) and induced ipsiversive turns (magenta) executed during training days 3 to 8 onto the same coordinate system. Black crosses mark the first bin with the first significant change in turning velocity following visual offset perturbation. Error bars indicate SEM over turns. Dashed black line marks line of unity.

SUPPLEMENTAL TABLES

	Total neurons recorded per mouse ± SEM	**Contraversive** neurons per mouse ± SEM	**Ipsiversive** neurons per mouse ± SEM
Layer 2/3 (8 mice)	144 ± 15	77 ± 14	67 ± 15
Layer 5 PT (11 mice)	51 ± 14	21 ± 8	30 ± 9
Layer 5 IT (9 mice)	34 ± 5	15 ± 3	19 ± 3

Table S1. Number of contraversive and ipsiversive neurons per mouse. Related to Figure 3.

Figures	Experiments	Sample size (*genotype*)
1C	Quantification of learning without and with optogenetic inhibition	**Control group (black):** n = 22 mice (3 *vGAT::ChR2(H134R)::EYFP*, 8 *vGAT-Cre* x *ROSA-LSL-tdTom*, 11 *Sim1-Cre(KJ18)*) **Optogenetics group (blue):** n = 12 mice (*vGAT::ChR2(H134R)::EYFP*)
1D	Performance testing without and with optogenetic inhibition	n = 15 mice (*vGAT::ChR2(H134R)::EYFP*)
2A-B, 2E-F	Quantification of turning behavior without optogenetic inhibition	n = 22 mice (3 *vGAT::ChR2(H134R)::EYFP*, 8 *vGAT-Cre* x *ROSA-LSL-tdTom*, 11 *Sim1-Cre(KJ18)*)
2C-D, 2G-H	Quantification of turning behavior with optogenetic inhibition	n = 14 (*vGAT::ChR2(H134R)::EYFP*)
3C-F, 4A-C, 5A, 6A-C, 7A-F, 8A	Quantification of turning related activity in layer 2/3 data set	n = 8 mice (*vGAT-Cre* x *ROSA-LSL-tdTom*) 1154 successively recorded neurons
3G-J, 4D-F, 5B, 6D-F, 7G-L, 8B	Quantification of turning related activity in layer 5 PT data set	n = 11 mice (*Sim1-Cre(KJ18)*), 560 successively recorded neurons
S1C-E	Additional quantification of learning impairment with optogenetic inhibition or chronic ibotenic acid lesions	**Control group (black):** n = 22 mice (3 *vGAT::ChR2(H134R)::EYFP*, 8 *vGAT-Cre* x *ROSA-LSL-tdTom*, 11 *Sim1-Cre(KJ18)*) **Optogenetics group (blue):** n = 12 mice (*vGAT::ChR2(H134R)::EYFP*) **Ibotenic acid group (brown):** n = 5 mice (*C57/BL6*)
S1F	Comparison of performance impairment in expert mice at two different stimulus locations in motor cortex	n = 9 mice (*vGAT::ChR2(H134R)::EYFP)*
S1H	Learning slope comparison without and with optogenetic inhibition	**Optogenetics groups (purple):** n = 3 mice (*vGAT::ChR(H134R)::EYFP*) **Control group (black):** n = 22 mice (3 *vGAT::ChR2(H134R)::EYFP*, 8 *vGAT-Cre* x *ROSA-LSL-tdTom*, 11 *Sim1-Cre(KJ18)*)
S1I	Quantification of learning in wild type mice with optogenetic stimulation	**Control group (black):** n = 22 mice (3 *vGAT::ChR2(H134R)::EYFP*, 8 *vGAT-Cre* x *ROSA-LSL-tdTom*, 11 *Sim1-Cre(KJ18)*) **Optogenetics group (orange):** n = 4 (*C57/Bl6*)

S2A-S2B	Quantification of induced turning behavior with and without chronic optogenetic inhibition	**Laser OFF group (left):** n = 3 (*vGAT::ChR(H134R)::EYFP*) **Laser ON group (right):** n = 12 (*vGAT::ChR(H134R)::EYFP*)
S2C-S2E	Quantification of behavior with and without timed optogenetic inhibition	n = 14 (*vGAT::ChR(H134R)::EYFP*)
S2F-I	Quantification of wild type turning behavior with optogenetic inhibition	n = 6 (*C57/Bl6*)
S3C-E	Comparison of layer 5 PT soma and dendrite activity	**Upper row:** n = 3 mice (*Sim1-Cre(KJ18)*) **Lower row:** n = 8 mice (*Sim1-Cre(KJ18)*)
S4A, S4C-E, S5A-B, S6A-F, S7A-B	Quantification of turning and running related activity in layer 2/3 data set	n = 8 mice (*vGAT-Cre* x *ROSA-LSL-tdTom*) 1154 successively recorded neurons
S4B, S4F-H, S5C-D, S6G-L, S7C-D	Quantification of turning and running related activity in layer 5 PT data set	n = 11 mice (*Sim1-Cre(KJ18)*), 560 successively recorded neurons
S7M	Quantification of learning related change in the number of target-directed turns	n = 19 mice (8 *vGAT-Cre* x *ROSA-LSL-tdTom*, 11 mice (*Sim1-Cre(KJ18)*)
S8	Quantification of main effects in layer 5 IT data set	n = 9 mice (*Tlx3-Cre(PL56)*), 308 successively recorded neurons

Table S2. Experiments and sample size reported in this manuscript. Related to STAR Methods.